Iteratively Learn Diverse Strategies with State Distance Information

Anonymous Author(s)
Affiliation
Address
`email`

Abstract

In complex reinforcement learning (RL) problems, policies with similar rewards may have substantially different behaviors. It remains a fundamental challenge to optimize rewards while also discovering as many *diverse* strategies as possible, which can be crucial in many practical applications. Our study examines two design choices for tackling this challenge, i.e., *diversity measure* and *computation framework*. First, we find that with existing diversity measures, visually indistinguishable policies can still yield high diversity scores. To accurately capture the behavioral difference, we propose to incorporate the state-space distance information into the diversity measure. In addition, we examine two common computation frameworks for this problem, i.e., population-based training (PBT) and iterative learning (ITR). We show that although PBT is the precise problem formulation, ITR can achieve comparable diversity scores with higher computation efficiency, leading to improved solution quality in practice. Based on our analysis, we further combine ITR with two tractable realizations of the state-distance-based diversity measures and develop a novel diversity-driven RL algorithm, *State-based Intrinsic-reward Policy Optimization* (SIPO), with provable convergence properties. We empirically examine SIPO across three domains from robot locomotion to multi-agent games. In all of our testing environments, SIPO consistently produces strategically diverse and human-interpretable policies that cannot be discovered by existing baselines.

1 Introduction

A consensus in deep learning (DL) is that different local optima have similar mappings in the functional space, leading to similar losses to the global optimum [57, 52, 36]. Hence, via stochastic gradient descent (SGD), most DL works only focus on the final performance without considering *which* local optimum SGD discovers. However, in complex reinforcement learning (RL) problems, the policies associated with different local optima can exhibit significantly different behaviors [9, 31, 59]. Thus, it is a fundamental problem for an RL algorithm to not only optimize rewards but also discover as many diverse strategies as possible. A pool of diversified policies can be further leveraged towards a wide range of applications, including the discovery of emergent behaviors [30, 2, 56], generating diverse dialogues [26], designing robust robots [11, 22, 17], and enhancing human-AI collaboration [34, 8, 10].

Obtaining diverse RL strategies requires a quantitative method for measuring the difference (i.e., *diversity*) between two policies. However, how to define such a measure remains an open challenge. Previous studies have proposed various diversity measures, such as comparing the difference between the action distributions generated by policies [55, 34, 69], computing probabilistic distances between the state occupancy of different policies [39], or measuring the mutual information between states and policy identities [14]. However, it remains unclear which measure could produce the best empirical performance. Besides, the potential pitfalls of these measures are rarely discussed.

Submitted to 37th Conference on Neural Information Processing Systems (NeurIPS 2023). Do not distribute.

In addition to diversity measures, there are two common computation frameworks for discovering diverse policies, including population-based training (PBT) and iterative learning (ITR). PBT directly solves a constrained optimization problem by learning a collection of policies simultaneously, subject to policy diversity constraints [48, 34, 8]. Although PBT is perhaps the most popular framework in the existing literature, it can be computationally challenging [44] since the number of constraints grows quadratically with the number of policies. The alternative framework is ITR, which iteratively learns a single policy that is sufficiently different from previous policies [39, 69]. ITR is a greedy relaxation of the PBT framework and it largely simplifies the optimization problem in each iteration. However, the performance of the ITR framework has not been theoretically analyzed yet, and it is often believed that ITR can be less efficient due to its sequential nature.

We provide a comprehensive study of the two aforementioned design choices. First, we examine the limitations of existing diversity measures in a few representative scenarios, where two policies outputting very different action distributions can still lead to similar state transitions. In these scenarios, state-occupancy-based measures are not sufficient to truly reflect the underlying behavior differences of the policies either. By contrast, we observe that diversity measures based on *state distances* can accurately capture the visual behavior differences of different policies. Therefore, we suggest that an effective diversity measure should explicitly incorporate state distance information for the best practical use. Furthermore, for the choice of computation framework, we conduct an in-depth analysis of PBT and ITR. We provide theoretical evidence that ITR, which has a simplified optimization process with fewer constraints, can discover solutions with the same reward as PBT while achieving *at least half* of the diversity score. This finding implies that although ITR is a greedy relaxation of PBT, their optimal solutions can indeed have comparable qualities. Furthermore, note that policy optimization is much simplified in ITR, which suggests that ITR can result in much better empirical performances and should be preferred in practice.

Following our insights, we combine ITR and a state-distance-based diversity measure to develop a generic and effective algorithm, *State-based Intrinsic-reward Policy Optimization (SIPO)*, for discovering diverse RL strategies. In each iteration, we further solve this constrained optimization problem via Lagrangian method and two-timescale gradient descent ascent (GDA) [27]. We theoretically prove that our algorithm is guaranteed to converge to a neighbor of ϵ-stationary point. Regarding the diversity measure, we provide two practical realizations, including a straightforward version based on the RBF kernel and a more general learning-based variant using Wasserstein distance.

We evaluate SIPO in three domains ranging from single-agent continuous control to multi-agent games: Humanoid locomotion [38], StarCraft Multi-Agent Challenge [53], and Google Research Football (GRF) [23]. Our findings demonstrate that SIPO surpasses baselines in terms of population diversity score across all three domains. Remarkably, our algorithm can successfully discover 6 distinct human-interpretable strategies in the GRF 3-vs-1 scenario and 4 strategies in two 11-player GRF scenarios, namely counter-attack and corner, without any domain-specific priors, which are beyond the capabilities of existing algorithms.

2 Related Work

Diversity in RL. It has been shown that policies trained under the same reward function can exhibit significantly different behaviors [9, 31]. Merely discovering a single high-performing solution may not suffice in various applications [11, 59, 22]. As such, the discovery of a diverse range of policies is a fundamental research problem, garnering attention over many years [40, 12, 24]. Early works are primarily based on multi-objective optimization [41, 51, 35, 43, 50], which assumes a set of reward functions is given in advance. In RL, this is also related to reward shaping [42, 1, 13, 56]. We consider learning diverse policies without any domain knowledge.

Population-based training (PBT) is the most popular framework for diverse solutions by jointly learning separate policies. Representative works include evolutionary computation [60, 33, 48], league training [59, 20], computing Hessian matrix [47] or constrained optimization with a population diversity measure [34, 68, 25, 32, 8]. An improvement is to learn a latent variable policy instead of separate ones. Prior works have incorporated different domain knowledge to design the latent code, such as action clustering [61], agent identities [25] or prosocial level [49, 2]. The latent variable can be also learned in an unsupervised fashion, such as in DIYAN [14] and its variants [22, 45]. Zahavy et al. [66] learns latent-conditioned diverse policies with hard constraints on rewards to ensure the derived policies are (nearly) optimal. In contrast, we prioritize diversity and fully accept sub-optimal strategies, leading to a hard constraint on diversity measures.

Iterative learning (ITR) simplifies PBT by only optimizing a single policy in each iteration and forcing it to behave differently w.r.t. previously learned ones [39, 55, 69]. While some ITR works require an expensive clustering process before each iteration [67] or domain-specific features [65], we consider domain-agnostic ITR in an end-to-end fashion. Besides, Pacchiano et al. [46] learns a kernel-based score function to iteratively guide policy optimization. The score function is conceptually similar to SIPO-WD but is applied to a parallel setting with more restricted expressiveness power.

Diversity Measure. Most previous works considered diversity measures on action distribution and state occupancy. For example, measures such as Jensen-Shannon divergence [34] and cross-entropy [69] are defined over policy distributions to encourage different policies to take different actions on the same state, implicitly promoting the generation of diverse trajectories. Other measures such as maximum mean discrepancy [39] maximize the probability distance between the state distributions induced by two policies. However, these approaches can fail to capture meaningful behavior differences between two policies in certain scenarios, as we will discuss in Section 4.1. There also exist specialized measures, such as cross-play rewards [8], which is designed for cooperative multi-agent games. It is worth noting that diversity measures are closely related to exploration criteria [3, 18, 5] and skill discovery [7, 28, 21], where a diversity surrogate objective is often introduced to encourage broad state coverage. However, this paper aims to explicitly discover mutually distinct policies. Our diversity measure depends on a function that computes the distance between states visited by two policies.

3 Preliminary

Notation: We consider POMDP [54] defined by $\mathcal{M} = \langle \mathcal{S}, \mathcal{A}, \mathcal{O}, r, P, O, \nu, H \rangle$. $\mathcal{S}$ is the state space. $\mathcal{A}$ and $\mathcal{O}$ are the action and observation space. $r : \mathcal{S} \times \mathcal{A} \to \mathbb{R}$ is the reward function. $O : \mathcal{S} \to \mathcal{O}$ is the observation function. H is the horizon. P is the transition function. At timestep h, the agent receives an observation $o_h = O(s_h)$ and outputs an action $a_h \in \mathcal{A}$ w.r.t. its policy $\pi : \mathcal{O} \to \triangle(\mathcal{A})$. The RL objective $J(\pi)$ is defined by $J(\pi) = \mathbb{E}_{(s_h,a_h)\sim(P,\pi)} \left[\sum_{h=1}^{H} r(s_h, a_h)\right]$. The above formulation can be naturally extended to cooperative multi-agent settings, where π and R correspond to the joint policy and the shared reward. Moreover, in this paper, we **assume access to object-centric information and features** rather than pure visual observations to simplify our discussion. We remark that although we restrict the scope of this paper to states, our method can be further extended to high-dimensional inputs (e.g. images, see App. B.3) via representation learning.

Finally, to discover diverse strategies, we aim to learn a set of M policies $\{\pi_i\}_{i=1}^{M}$ such that all of these policies are locally optimal under $J(\cdot)$ but mutually distinct subject to some diversity measure $D(\cdot,\cdot) : \triangle \times \triangle \to \mathbb{R}$, which captures the difference between two policies.

Existing Diversity Measures: We say a diversity measure D is defined over action distribution if it can be written as

$$D(\pi_i, \pi_j) = \mathbb{E}_{s\sim q(s)} \left[\tilde{D}_{\mathcal{A}} \left(\pi_i(\cdot \mid s) \| \pi_j(\cdot \mid s)\right)\right], \tag{1}$$

where q is an occupancy measure over states, $\tilde{D}_{\mathcal{A}} : \triangle \times \triangle \to \mathbb{R}$ measures the difference between action distributions. $\tilde{D}_{\mathcal{A}}$ can be any probability distance as defined in prior works [55, 34, 69, 48].

Denote the state occupancy of π as q_π. We say a diversity measure is defined over state occupancy if it can be written as

$$D(\pi_i, \pi_j) = \tilde{D}_{\mathcal{S}} \left(q_{\pi_i} \| q_{\pi_j}\right), \tag{2}$$

which can be realized as an integral probability metric [39]. We remark that q_π is usually intractable.

In addition to diversity measures, we present two popular computation frameworks for this purpose.

Population-Based Training (PBT): PBT is a straightforward formulation by jointly learning M policies $\{\pi_i\}_{i=1}^{M}$ subject to pairwise diversity constraints, i.e.,

$$\max_{\{\pi_i\}} \sum_{i=1}^{M} J(\pi_i) \;\text{ s.t. } D(\pi_j, \pi_k) \geq \delta, \forall j, k \in [M],\, j \neq k, \tag{3}$$

where δ is a threshold. In our paper, we consistently refer to the aforementioned computation framework as "PBT", rather than adjusting hyperparameters [19]. Despite a precise formulation, PBT poses severe optimization challenges due to mutual constraints.

Table 1: Diversity measures of the grid-world example. Computation details can be found in App. B.

	human	action-based				state-distance-based	
		KL	JSD$_1$	JSD$_0$/EMD	L_2 norm	L_2 norm	EMD
$D(\pi_1, \pi_2)$	small	$+\infty$	$\mathbf{\log 2}$	$\mathbf{1/2}$	$\mathbf{\sqrt{7}}$	$2\sqrt{2}$	5.7
$D(\pi_1, \pi_3)$	large	$+\infty$	$\mathbf{\log 2}$	$1/8$	1	$\mathbf{2\sqrt{6}}$	**11.3**

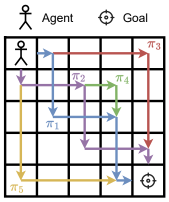

Figure 1: (left) A grid-world environment with 5 different optimal policies. Intuitively, $D(\pi_1, \pi_2) < D(\pi_1, \pi_3)$ and $D(\pi_3, \pi_4) < D(\pi_3, \pi_5)$. However, action-based measures can give $D_{\mathcal{A}}(\pi_1, \pi_2) \geq D_{\mathcal{A}}(\pi_1, \pi_3)$ and state-occupancy-based measures can give $D(\pi_3, \pi_4) = D(\pi_3, \pi_5)$.

Iterative Learning (ITR): ITR is a greedy approximation of PBT by iteratively learning novel policies. In the i-th ($1 \leq i \leq M$) iteration, ITR solves

$$\pi_i^\star = \arg\max_{\pi_i} J(\pi_i) \;\; \text{s.t.}\; D(\pi_i, \pi_j^\star) \geq \delta, \forall 1 \leq j < i. \tag{4}$$

$\pi_j^\star$ is recursively defined by the above equation. Compared with PBT, ITR trades off wall-clock time for less required computation resources (e.g., GPU memory) and performs open-ended training (i.e., the population size M does not need to be fixed at the beginning of training).

4 Analysis of Existing Diversity-Discovery Approaches

In this section, we conduct both quantitative and theoretical analyses of existing approaches to motivate our method. We first discuss diversity measures in Sec. 4.1 and then compare computation frameworks, namely PBT and ITR, in Sec. 4.2.

4.1 A Common Missing Piece in Diversity Measure: State Distance

The perception of diversity among humans primarily relies on the level of dissimilarity within the state space, which is measured by a distance function. However, the diversity measures outlined in Eq. (1) and Eq. (2) completely fail to account for such crucial information. In this section, we provide a detailed analysis to instantiate this observation with concrete examples and propose a novel diversity measure defined over state distances.

First, we present a synthetic example to demonstrate the limitations of current diversity measures. Our example consists of a grid-world environment with a single agent and grid size N_G. The agent starts at the top left of the grid-world and must navigate to the bottom right corner, as shown in Fig. 1. While N_G can be large in general, we illustrate with $N_G = 5$ for simplicity. We draw five distinct policies, denoted as π_1 through π_5, which differ in their approach to navigating the grid-world. Consider π_1, π_2, and π_3 first. Although humans may intuitively perceive that policies π_1 and π_2, which move along the diagonal, are more similar to each other than to π_3, which moves along the boundary, diversity measures based on actions can fail to reflect this intuition, as shown in Table 1. Then, let's switch to policies π_3, π_4, and π_5. We find that state-occupancy-based diversity measures are unable to differentiate between π_4 and π_5 in contrast to π_3. This is because the states visited by π_3 are entirely disjoint from those visited by both π_4 and π_5. However, humans would judge π_5 to be more distinct from π_3 than π_4 because both π_3 and π_4 tend to visit the upper boundary.

Next, we consider a more realistic and complicated multi-agent football scenario in Fig. 2, where an idle player in the backyard takes an arbitrary action without involving in the attack at all. Although the idle player stays still with no effect on the team strategy, action-based measures can produce high diversity scores when the idle player takes different duplicated actions.

To summarize, existing measures suffer from a significant limitation — they only compare the behavior trajectories *implicitly* through the lens of action or state distribution without *explicitly measuring state distance*. Specifically, action-based measures fail to capture the behavioral differences that may arise when similar states are reached via different actions. Similarly, state occupancy measures do not quantify *the degree of dissimilarity* between states. To address this limitation, we propose a new diversity measure that explicitly takes into account the distance function in state space:

$$D(\pi_i, \pi_j) = \mathbb{E}_{(s,s') \sim \gamma}\left[g\left(d\left(s, s'\right)\right)\right], \tag{5}$$

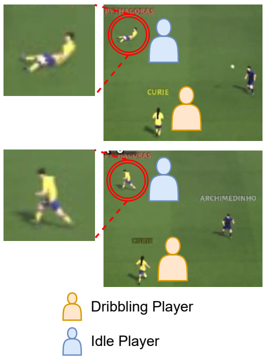

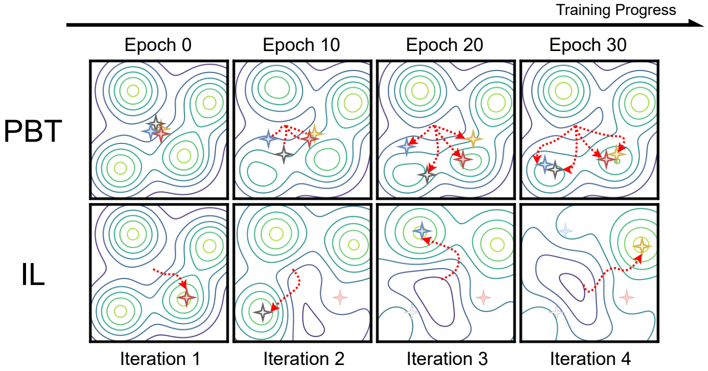

Figure 2: Duplicate actions in multi-agent football. For players who are not involved in the attack, actions like "pass", "shoot", and "slide" result in the same consequence. Diversity measures should not focus on these actions.

Figure 3: Illustration of the learning process of PBT and ITR in a 2-D navigation environment with 4 modes. PBT will not uniformly converge to different landmarks as computation can be either too costly or unstable. By contrast, ITR repeatedly excludes a particular landmark, such that policy in the next iteration can continuously explore until a novel landmark is discovered.

d is a distance metric over $\mathcal{S} \times \mathcal{S}$. $g : \mathbb{R}^+ \to \mathbb{R}$ is a monotonic cost function. $\gamma \in \Gamma(q_{\pi_i}, q_{\pi_j})$ is a distribution over state pairs. $\Gamma(q_{\pi_i}, q_{\pi_j})$ denotes the collection of all distributions on $\mathcal{S} \times \mathcal{S}$ with marginals q_{π_i} and q_{π_j} on the first and second factors respectively. We also note that states are consequences of performed actions. Hence, a state-distance-based measure also implicitly reflects the (meaningful) differences in actions between two policies. We compute two simple measures based on state distance, i.e., the L_2 norm and the Earth Moving Distance (EMD), for the grid-world example and present results in Table 1. These measures are consistent with human intuition.

4.2 Computation Framework: Population-Based or Iterative Learning?

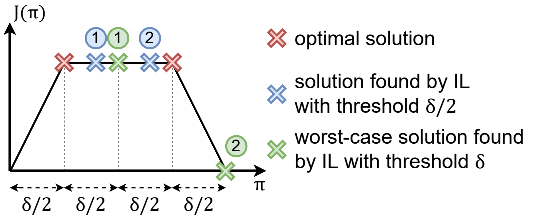
J(π)
①
①
②
optimal solution
solution found by IL with threshold δ/2
②
worst-case solution found by IL with threshold δ
π
δ/2
δ/2
δ/2
δ/2

Figure 4: 1-D worst case of IL. With threshold δ, IL finds solutions with inferior rewards. However, IL can find optimal solutions if the threshold is halved.

We first consider a simplest motivating example to intuitively illustrate the optimization challenges. Let's assume that π_i is a scalar, $J(\pi_i)$ is linear in π_i, and $D(\pi_i, \pi_j) = |\pi_i - \pi_j|$. In our definition, where M denotes the number of diverse policies, PBT involves $\Theta(M^2)$ constraints in a single linear programming problem while ITR involves $\mathcal{O}(M)$ constraints in each of M iterations. Given that the complexity of linear programming is a high-degree polynomial (higher than 2) of the number of constraints, solving PBT is harder (and probably slower) than solving ITR in a total of M iterations, *despite PBT being parallelized*. This challenge can be more severe in RL due to complex solution space and large training variance.

Although ITR can be optimized efficiently, it remains unclear whether ITR, as a greedy approximation of PBT, can obtain solutions of comparable rewards. Fig. 4 shows the worst case in the 1-D setting when the ITR solutions (green) can indeed have lower rewards than the PBT solution (red) subject to the same diversity constraint. However, we will show in the next theorem that ITR is guaranteed to have no worse rewards than PBT by trading off half of the diversity.

Theorem 4.1. *Assume D is a distance metric. Denote the optimal value of Eq.(3) as T_1. Let $T_2 = \sum_{i=1}^{M} J(\tilde{\pi}_i)$ where*

$$\tilde{\pi}_i = \arg\max_{\pi_i} J(\pi_i) \;\; s.t. \;\; D(\pi_i, \tilde{\pi}_j) \geq \delta/2, \forall 1 \leq j < i \tag{6}$$

for $i = 1, \ldots, M$, then $T_2 \geq T_1$.

Please see App. E.1 for the proof. The above theorem provides a quality guarantee for ITR. The proof can be intuitively explained by the 1-D example in Fig. 4, where green points represent the worst case with threshold δ and blue points represent the solutions with threshold $\delta/2$. Thm. 4.1 shows that, for any policy pool derived by PBT, we can always use ITR to obtain another policy pool, which has *the same rewards* and *comparable diversity scores*.

Empirical Results: We empirically compare PBT and ITR in a 2-D navigation environment with 1 agent and N_L landmarks in Fig. 3. The reward is 1 if the agent successfully navigates to a landmark and 0 otherwise. We train N_L policies using both PBT and ITR to discover strategies toward each of these landmarks. More details can be found in App. D. Table 2 shows the number of discovered landmarks by PBT and ITR. ITR performs consistently better than PBT even in this simple example. We intuitively illustrate the learning process of PBT and ITR in Fig. 3. ITR, due to its computation efficiency, can afford to run longer iterations and tolerate larger exploration noises. Hence, it can converge easily to diverse solutions by imposing a large diversity constraint. PBT, however, only converges when the exploration is faint, otherwise it diverges or converges too slowly.

Table 2: The number of discovered landmarks across 6 seeds with standard deviation in the bracket.

setting	PBT	ITR
$N_L = 4$	2.0 (1.0)	**3.5** (0.5)
$N_L = 5$	2.2 (0.9)	**4.5** (0.5)

4.3 Practical Remark

Based on the above analyses, we suggest ITR and diversity measures based on state distances be *preferred* in RL applications. We also acknowledge that, by the no-free-lunch theorem, they cannot be universal solutions and that trade-offs may still exist (see discussions in Sec.7 and App.F). Nonetheless, in the following sections, we will show that the effective implementation of these choices can lead to superior performances in various challenging benchmarks. We hope that our approach will serve as a starting point and provide valuable insights into the development of increasingly powerful algorithms for potentially more challenging scenarios.

5 Method

In this section, we develop a diversity-driven RL algorithm, *State-based Intrinsic-reward Policy Optimization (SIPO)*, by combining ITR and state-distance-based measures. SIPO runs M iterations to discover M distinct policies. At the i-th iteration, we solve equation (4) by converting it into unconstrained optimization using the Lagrange method. The unconstrained optimization can be written as:

$$\min_{\pi_i} \max_{\lambda_j \geq 0,\, 1 \leq j < i} -J(\pi_i) - \sum_{j=1}^{i-1} \lambda_j \left(D_{\mathcal{S}}(\pi_i, \pi_j^\star) - \delta \right) \tag{7}$$

λ_j $(1 \leq j < i)$ are Lagrange multipliers. $\{\pi_j^\star\}_{j=1}^{i-1}$ are previously obtained policies. We adopt two-timescale Gradient Descent Ascent (GDA) [27] to solve the above minimax optimization, i.e., performing gradient descent over π_i and gradient ascent over λ_j with different learning rates. In our algorithm, we additionally enforce the dual variables λ_j to be bounded (i.e., in an interval $[0, \Lambda]$ for a large number Λ), which plays an important role both in the theoretical analysis and in empirical convergence. However, $D_{\mathcal{S}}(\pi_i, \pi_j^\star)$ cannot be directly optimized w.r.t. π_i through gradient-based methods because it is related to the states visited by π_i. We cast $D_{\mathcal{S}}(\pi_i, \pi_j^\star)$ as intrinsic rewards and optimize the joint return via policy gradient. The pseudocode of SIPO can be found in App. G.

An important property of SIPO is the convergence guarantee. We present an informal illustration in Thm. 5.1 and present the formal theorem with proof in App. E.2.

Theorem 5.1. *(Informal) Under continuity assumptions, SIPO converges to an ϵ-stationary point.*

Remark: We assumed that the return J and the distance $D_{\mathcal{S}}$ are smooth in policies. In practice, this is true if (1) policy and state space are bounded and (2) reward function and system dynamics are continuous in the policy. (Continuous functions are bounded over compact spaces.) The key step is to analyze the role of the bounded dual variables λ, which achieves an $\frac{1}{\Lambda}$-approximation of constraint without hurting the optimality condition.

Instead of directly defining $D_{\mathcal{S}}$, we define intrinsic rewards as illustrated in Sec. 5, such that $D_{\mathcal{S}}(\pi_i, \pi_j^\star) = \mathbb{E}_{s_h \sim \mu_{\pi_i}} \left[\sum_{h=1}^{H} r_{\text{int}}(s_h; \pi_i, \pi_j^\star) \right]$.

RBF Kernel: The most popular realization of Eq. (5) in machine learning is through kernel functions. Herein, we realize Eq. (5) as an RBF kernel on states. Formally, the intrinsic reward is defined by

$$r_{\text{int}}^{\text{RBF}}(s_h; \pi_i, \pi_j^\star) = \frac{1}{H} \mathbb{E}_{s' \sim \mu_{\pi_j^\star}} \left[-\exp\left(-\frac{\|s_h - s'\|^2}{2\sigma^2} \right) \right] \tag{8}$$

where σ is a hyperparameter controlling the variance.

Wasserstein Distance: For stronger discrimination power, we can also realize Eq. (5) as L_2-Wasserstein distance. According to the dual form [58], we define

$$r_{\text{int}}^{\text{WD}}(s_h;\pi_i,\pi_j^\star)=\frac{1}{H}\sup_{\|f\|_L\le 1} f(s_h)-\mathbb{E}_{s'\sim\mu_{\pi_j^\star}}\left[f(s')\right] \tag{9}$$

where $f:\mathcal{S}\to\mathbb{R}$ is a 1-Lipschitz function. We implement f as a neural network and clip parameters to $[-0.01, 0.01]$ to ensure the Lipschitz constraint. Note that $r_{\text{int}}^{\text{WD}}$ incorporates representation learning by utilizing a learnable scoring function f and is more flexible in practice. We also show in App. B.3 that $r_{\text{int}}^{\text{WD}}$ is robust to different inputs, including states with random noises and RGB images.

We name SIPO with $r_{\text{int}}^{\text{RBF}}$ and $r_{\text{int}}^{\text{WD}}$ ***SIPO-RBF*** and ***SIPO-WD*** respectively.

Implementation: To incorporate temporal information, we stack the recent 4 global states to compute intrinsic rewards and normalize the intrinsic rewards to stabilize training. In multi-agent environments, we learn an agent-ID-conditioned policy [15] and share the parameter across all agents. Our implementation is based on MAPPO [64] with more details in App. D.

6 Experiments

We evaluate SIPO across three domains that exhibit multi-modality of solutions. The first domain is the humanoid locomotion task in Isaac Gym [38], where diversity can be quantitatively assessed by well-defined behavior descriptors. We remark that the issues we addressed in Sec. 4.1 may not be present in this task where the action space is small and actions are highly correlated with states. Further, we examine the effectiveness of SIPO in two much more challenging multi-agent domains, StarCarft Multi-Agent Challenge (SMAC) [53] and Google Research Football (GRF) [23], where well-defined behavior descriptors are not available and existing diversity measures may produce misleading diversity scores. We provide introductions to these environments in App. C.

First, we show that SIPO can efficiently learn diverse strategies and outperform several baseline methods, including DIPG [39], SMERL [22], DvD [48], and RSPO [69]. Then, we qualitatively demonstrate the emergent behaviors learned by SIPO, which are both *visually distinguishable* and *human-interpretable*. Finally, we perform an ablation study over the building components of SIPO and show that both the diversity measure, ITR, and GDA are critical to the performance.

All algorithms run for the same number of environment frames on a desktop machine with an RTX3090 GPU. Numbers are average values over 5 seeds in Humanoid and SMAC and 3 seeds in GRF with standard deviation shown in brackets. More algorithm details can be found in App. D. Additional visualization results can be found in our project website (see App. A).

6.1 Comparison with Baseline Methods

Humanoid Locomotion. Following Zhou et al. [69], we train a population of size 4. We assess diversity by the pairwise distance of joint torques, a widely used behavior descriptor in recent Quality-Diversity works [62]. Torque states are not included as the input of diversity measures and we only use them for evaluation to ensure a fair comparison. Results are shown in Table 3. We can see that both variants of SIPO can outperform all baseline methods except that SIPO-RBF achieves comparable performance with RSPO, even if RSPO explicitly encourages the output of different actions/forces.

Table 3: Pairwise distance of joint torques (i.e., diversity scores) in the humanoid locomotion task.

SIPO-RBF	SIPO-WD	RSPO
0.53(0.17)	**0.71(0.23)**	0.53(0.05)

DIPG	DvD	SMERL
0.12(0.04)	0.40(0.22)	0.01(0.00)

SMAC Following Zhou et al. [69], we run SIPO and all baselines on an easy map, *2m_vs_1z*, and a hard map, *2c_vs_64zg*, both across 4 iterations. We merge all trajectories produced by the policy collection and incorporate a k-nearest-neighbor state entropy estimation [28] to assess diversity. Intuitively, a more diverse population should have a larger state entropy value. We set $k = 12$ following Liu and Abbeel [28] and show results in Table 4. On these maps, two agents are both involved in the attack. Therefore, RSPO, which incorporates an action-based cross-entropy measure, can perform well across all baselines. However, SIPO explicitly compares the distance between resulting trajectories and can even outperform RSPO, leading to the most diverse population.

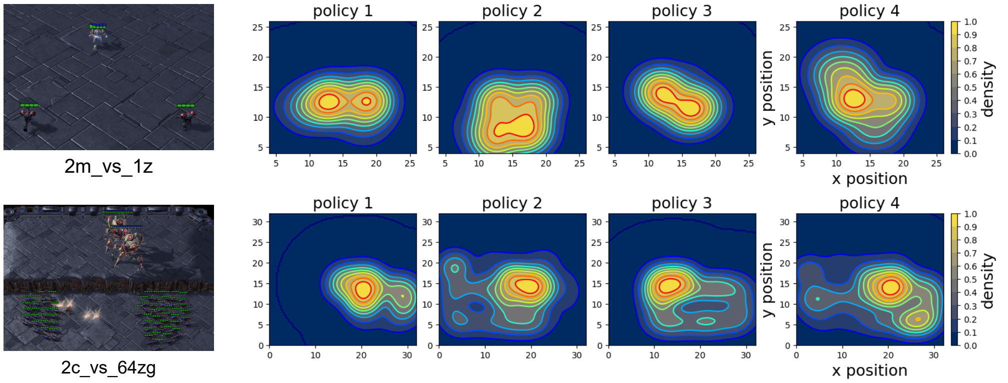

Figure 5: Heatmaps of agent positions in SMAC across 4 iterations with SIPO-RBF.

GRF We consider three academy scenarios, specifically *3v1*, *counterattack* (*CA*), and *corner*. The GRF environment is more challenging than SMAC due to the large action space, more agents, and the existence of duplicate actions. We determine a population size $M = 4$ by balancing resources and wall-clock time across different baselines. Table 5 compares the number of distinct policies (in terms of ball-passing routes, see App. B.2) discovered in the population. Due to the strong adversarial power of our diversity measures and the application of GDA, SIPO is the most efficient and robust — even in the challenging 11-vs-11 *corner* and *CA* scenario, SIPO can effectively discover different winning strategies in just a few iterations across different seeds. By contrast, baselines suffer from learning instability in these challenging environments and tend to discover policies with slight distinctions. We also calculate the estimated state entropy as we did in SMAC. However, we find that this metric cannot distinguish fine-grained ball-passing behaviors in GRF (check our discussions in App. B).

Remark: In GRF experiments, when M is small, even repeated training with different random seeds (PG) is a strong baseline (see Table 5). Hence, the numbers are actually restricted in a small interval (with a lower bound equal to PG results and an upper bound equal to $M = 4$), which makes the improvements by SIPO seemingly less significant. However, achieving clear improvements in these challenging applications remains particularly non-trivial. With a population size $M = 10$, SIPO clearly outperforms baselines by consistently discovering one or more additional strategies.

Table 4: State entropy estimated by k-nearest-neighbor in SMAC. ($k = 12$)

	2m_vs_1z	*2c_vs_64zg*
SIPO-RBF	**0.038(0.002)**	**0.072(0.003)**
SIPO-WD	0.036(0.001)	0.056(0.003)
RSPO	0.032(0.003)	0.070(0.001)
DIPG	0.032(0.002)	0.056(0.004)
SMERL	0.028(0.002)	0.042(0.002)
DvD	0.030(0.002)	0.057(0.003)

6.2 Qualitative Analysis

For SMAC, we present heatmaps of agent positions in Fig. 5. The heatmaps clearly show that SIPO can consistently learn novel winning strategies to conquer the enemy. Fig. 6 presents the learned behavior by SIPO in the GRF *3v1* scenario of seed 1. We can observe that agents have learned a wide spectrum of collaboration strategies across merely 7 iterations. The strategies discovered by SIPO are both *diverse* and *human-interpretable*. In the first iteration, all agents are involved in the attack such that they can distract the defender and obtain a high win rate. The 2nd and the 6th iteration demonstrate an efficient pass-and-shoot strategy, where agents quickly elude the defender and score a goal. In the 3rd and the 7th iterations, agents learn smart "one-two" strategies to bypass the defender, a prevalent tactic employed by human football players. We note that *NONE* of the baselines have

Table 5: Number of distinct strategies in GRF discovered by different methods in terms of the ball-passing route. Details of the evaluation protocol can be found in App. B.2.

	Population Size M	ours		baselines				random
		SIPO-RBF	SIPO-WD	DIPG	SMERL	DvD[1]	RSPO	PG
3v1	4	**3.0 (0.8)**	**3.0 (0.0)**	2.7 (0.5)	1.3 (0.5)	**3.0 (0.8)**	2.0 (0.0)	2.7 (0.5)
CA	4	**3.3 (0.5)**	3.0 (0.8)	2.3 (0.5)	1.3 (0.5)	-	2.0 (0.0)	1.7 (0.5)
corner	4	2.7 (0.5)	**3.0 (0.8)**	1.7 (0.5)	1.0 (0.0)	-	1.6 (0.5)	2.0 (0.8)
3v1	10	4.3 (0.5)	**5.7 (0.5)**	3.7 (0.5)	-	-	2.3 (0.5)	-

[1] Training DvD in *CA* and *corner* or with $M = 10$ requires >24GB GPU memory, which exceeds our memory limit.

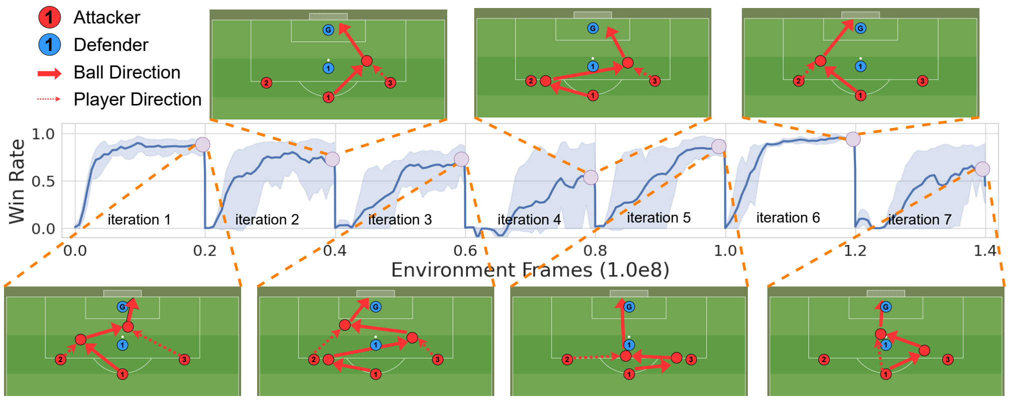

Figure 6: Learning curves and discovered strategies by SIPO-WD in the *3v1* scenario over 7 iterations. Strategies of seed 1 are shown.

ever discovered this strategy across all runs, while SIPO is consistently able to derive such strategies for all random seeds. Visualization results in *CA* and *corner* scenarios can be found in App. B.

6.3 Ablation Study

We apply these changes to SIPO-WD:

- *fix-L*: Fixing the multiplier λ_i instead of applying GDA.
- *CE*: The intrinsic reward is replaced with cross-entropy, i.e., $r_{\text{int}}^{\text{CE}}(s_h, a_h) = -\log \pi_j^\star(a_h \mid s_h)$, where $\pi_j^\star$ denotes a previously discovered policy. Additionally, GDA is still applied.
- *filter*: Optimizing the extrinsic rewards on trajectories that have intrinsic returns exceeding δ and optimizing intrinsic rewards defined by Eq. (9) for other trajectories [69].
- *PBT*: Simultaneously training M policies with $M(M-1)/2$ constraints (i.e., directly solving Eq. (3)) with intrinsic rewards defined by Eq. (9) and GDA.

Table 6: # distinct strategies of ablations in GRF.

	ours	fix-L	CE	filter	PBT
3v1	**3.0 (0.0)**	1.0 (0.0)	2.7 (0.5)	1.3 (0.5)	2.7 (0.5)
CA	**3.0 (0.8)**	-^{1}	2.3 (0.8)	1.0 (0.0)	-^{2}
corner	**3.0 (0.8)**	-^{1}	1.7 (0.5)	1.0 (0.0)	-^{2}

^{1} Not converged.
^{2} Training requires >24GB memory and exceeds our memory limit.

We report the number of visually distinct policies discovered by these methods in Table 6. Comparison between SIPO and CE demonstrates that the action-based cross-entropy measure may suffer from duplicate actions in GRF and produce nearly identical behavior by overly exploiting duplicate actions, especially in the *CA* and *corner* scenarios with 11 agents. Besides, the fixed Lagrange coefficient, the filtering-based method, and PBT are all detrimental to our algorithm. These methods also suffer from significant training instability. Overall, the state-distance-based diversity measure, ITR, and GDA are all critical to the performance of SIPO.

7 Conclusion

We tackle the problem of discovering diverse high-reward policies in RL. First, we demonstrate concrete failure cases of existing diversity measures and propose a novel measure that explicitly compares the distance in state space. Next, we present a thorough comparison between PBT and ITR, and show that ITR is much easier to optimize and can derive solutions with comparable quality to PBT. Motivated by these insights, we combine ITR with a state-distance-based diversity measure to develop SIPO, which has provable convergence and can efficiently discover a wide spectrum of human-interpretable strategies in a wide range of environments.

Limitations: First, we assume direct access to an object-centric state representation. When such a representation is not available (e.g., image-based observations), representation learning becomes necessary and algorithm performance can be affected by the quality of the learned representations. Second, because ITR requires sequential training, the wall clock time of SIPO can be longer than the PBT alternatives when fixing the total number of training samples. The acceleration of ITR remains an open challenge.

References

[1] Monica Babes, Enrique Munoz de Cote, and Michael L. Littman. Social reward shaping in the prisoner's dilemma. In Lin Padgham, David C. Parkes, Jörg P. Müller, and Simon Parsons, editors, *7th International Joint Conference on Autonomous Agents and Multiagent Systems (AAMAS 2008), Estoril, Portugal, May 12-16, 2008, Volume 3*, pages 1389–1392. IFAAMAS, 2008. URL `https://dl.acm.org/citation.cfm?id=1402880`.

[2] Bowen Baker, Ingmar Kanitscheider, Todor M. Markov, Yi Wu, Glenn Powell, Bob McGrew, and Igor Mordatch. Emergent tool use from multi-agent autocurricula. In *8th International Conference on Learning Representations, ICLR 2020, Addis Ababa, Ethiopia, April 26-30, 2020*. OpenReview.net, 2020. URL `https://openreview.net/forum?id=SkxpxJBKwS`.

[3] Marc Bellemare, Sriram Srinivasan, Georg Ostrovski, Tom Schaul, David Saxton, and Remi Munos. Unifying count-based exploration and intrinsic motivation. *Advances in neural information processing systems*, 29, 2016.

[4] Yura Burda and Harri Edwards, Oct 2018. URL `https://openai.com/blog/reinforcement-learning-with-prediction-based-rewards/`.

[5] Yuri Burda, Harrison Edwards, Amos Storkey, and Oleg Klimov. Exploration by random network distillation. *arXiv preprint arXiv:1810.12894*, 2018.

[6] Andres Campero, Roberta Raileanu, Heinrich Küttler, Joshua B. Tenenbaum, Tim Rocktäschel, and Edward Grefenstette. Learning with amigo: Adversarially motivated intrinsic goals. In *9th International Conference on Learning Representations, ICLR 2021, Virtual Event, Austria, May 3-7, 2021*. OpenReview.net, 2021. URL `https://openreview.net/forum?id=ETBc_MIMgoX`.

[7] Víctor Campos, Alexander Trott, Caiming Xiong, Richard Socher, Xavier Giró-i Nieto, and Jordi Torres. Explore, discover and learn: Unsupervised discovery of state-covering skills. In *International Conference on Machine Learning*, pages 1317–1327. PMLR, 2020.

[8] Rujikorn Charakorn, Poramate Manoonpong, and Nat Dilokthanakul. Generating diverse cooperative agents by learning incompatible policies. In *ICML 2022 Workshop AI for Agent-Based Modelling*, 2022.

[9] Jack Clark and Dario Amodei, Dec 2016. URL `https://openai.com/blog/faulty-reward-functions/`.

[10] Brandon Cui, Andrei Lupu, Samuel Sokota, Hengyuan Hu, David J Wu, and Jakob Nicolaus Foerster. Adversarial diversity in hanabi. In *The Eleventh International Conference on Learning Representations*, 2023.

[11] Antoine Cully, Jeff Clune, Danesh Tarapore, and Jean-Baptiste Mouret. Robots that can adapt like animals. *Nature*, 521(7553):503–507, May 2015. ISSN 0028-0836, 1476-4687. doi: 10.1038/nature14422. URL `http://www.nature.com/articles/nature14422`.

[12] Kalyanmoy Deb and Amit Saha. Finding multiple solutions for multimodal optimization problems using a multi-objective evolutionary approach. In Martin Pelikan and Jürgen Branke, editors, *Genetic and Evolutionary Computation Conference, GECCO 2010, Proceedings, Portland, Oregon, USA, July 7-11, 2010*, pages 447–454. ACM, 2010. doi: 10.1145/1830483.1830568. URL `https://doi.org/10.1145/1830483.1830568`.

[13] Sam Devlin and Daniel Kudenko. Theoretical considerations of potential-based reward shaping for multi-agent systems. In Liz Sonenberg, Peter Stone, Kagan Tumer, and Pinar Yolum, editors, *10th International Conference on Autonomous Agents and Multiagent Systems (AAMAS 2011), Taipei, Taiwan, May 2-6, 2011, Volume 1-3*, pages 225–232. IFAAMAS, 2011. URL `http://portal.acm.org/citation.cfm?id=2030503&CFID=69153967&CFTOKEN=38069692`.

[14] Benjamin Eysenbach, Abhishek Gupta, Julian Ibarz, and Sergey Levine. Diversity is all you need: Learning skills without a reward function. In *7th International Conference on Learning Representations, ICLR 2019, New Orleans, LA, USA, May 6-9, 2019*. OpenReview.net, 2019. URL `https://openreview.net/forum?id=SJx63jRqFm`.

[15] Wei Fu, Chao Yu, Zelai Xu, Jiaqi Yang, and Yi Wu. Revisiting some common practices in cooperative multi-agent reinforcement learning. In Kamalika Chaudhuri, Stefanie Jegelka, Le Song, Csaba Szepesvari, Gang Niu, and Sivan Sabato, editors, *Proceedings of the 39th International Conference on Machine Learning*, volume 162 of *Proceedings of Machine Learning Research*, pages 6863–6877. PMLR, 17–23 Jul 2022. URL `https://proceedings.mlr.press/v162/fu22d.html`.

[16] Dibya Ghosh, Abhishek Gupta, and Sergey Levine. Learning actionable representations with goal conditioned policies. In *7th International Conference on Learning Representations, ICLR 2019, New Orleans, LA, USA, May 6-9, 2019*. OpenReview.net, 2019. URL `https://openreview.net/forum?id=Hye9lnCct7`.

[17] Agrim Gupta, Silvio Savarese, Surya Ganguli, and Li Fei-Fei. Embodied intelligence via learning and evolution. *Nature communications*, 12(1):1–12, 2021.

[18] Elad Hazan, Sham Kakade, Karan Singh, and Abby Van Soest. Provably efficient maximum entropy exploration. In *International Conference on Machine Learning*, pages 2681–2691. PMLR, 2019.

[19] Max Jaderberg, Valentin Dalibard, Simon Osindero, Wojciech M. Czarnecki, Jeff Donahue, Ali Razavi, Oriol Vinyals, Tim Green, Iain Dunning, Karen Simonyan, Chrisantha Fernando, and Koray Kavukcuoglu. Population Based Training of Neural Networks, November 2017. URL `http://arxiv.org/abs/1711.09846`. arXiv:1711.09846 [cs].

[20] Max Jaderberg, Wojciech M. Czarnecki, Iain Dunning, Luke Marris, Guy Lever, Antonio Garcia Castañeda, Charles Beattie, Neil C. Rabinowitz, Ari S. Morcos, Avraham Ruderman, Nicolas Sonnerat, Tim Green, Louise Deason, Joel Z. Leibo, David Silver, Demis Hassabis, Koray Kavukcuoglu, and Thore Graepel. Human-level performance in 3D multiplayer games with population-based reinforcement learning. *Science*, 364(6443):859–865, May 2019. ISSN 0036-8075, 1095-9203. doi: 10.1126/science.aau6249. URL `https://www.science.org/doi/10.1126/science.aau6249`.

[21] Zheyuan Jiang, Jingyue Gao, and Jianyu Chen. Unsupervised skill discovery via recurrent skill training. *Advances in Neural Information Processing Systems*, 35:39034–39046, 2022.

[22] Saurabh Kumar, Aviral Kumar, Sergey Levine, and Chelsea Finn. One solution is not all you need: Few-shot extrapolation via structured maxent RL. In Hugo Larochelle, Marc'Aurelio Ranzato, Raia Hadsell, Maria-Florina Balcan, and Hsuan-Tien Lin, editors, *Advances in Neural Information Processing Systems 33: Annual Conference on Neural Information Processing Systems 2020, NeurIPS 2020, December 6-12, 2020, virtual*, 2020. URL `https://proceedings.neurips.cc/paper/2020/hash/5d151d1059a6281335a10732fc49620e-Abstract.html`.

[23] Karol Kurach, Anton Raichuk, Piotr Stanczyk, Michal Zajac, Olivier Bachem, Lasse Espeholt, Carlos Riquelme, Damien Vincent, Marcin Michalski, Olivier Bousquet, and Sylvain Gelly. Google research football: A novel reinforcement learning environment. In *The Thirty-Fourth AAAI Conference on Artificial Intelligence, AAAI 2020, The Thirty-Second Innovative Applications of Artificial Intelligence Conference, IAAI 2020, The Tenth AAAI Symposium on Educational Advances in Artificial Intelligence, EAAI 2020, New York, NY, USA, February 7-12, 2020*, pages 4501–4510. AAAI Press, 2020. URL `https://ojs.aaai.org/index.php/AAAI/article/view/5878`.

[24] Yoonho Lee, Huaxiu Yao, and Chelsea Finn. Diversify and disambiguate: Learning from underspecified data. *CoRR*, abs/2202.03418, 2022. URL `https://arxiv.org/abs/2202.03418`.

[25] Chenghao Li, Tonghan Wang, Chengjie Wu, Qianchuan Zhao, Jun Yang, and Chongjie Zhang. Celebrating diversity in shared multi-agent reinforcement learning. In Marc'Aurelio Ranzato, Alina Beygelzimer, Yann N. Dauphin, Percy Liang, and Jennifer Wortman Vaughan, editors, *Advances in Neural Information Processing Systems 34: Annual Conference on Neural Information Processing Systems 2021, NeurIPS 2021, December 6-14, 2021, virtual*, pages 3991–4002, 2021. URL `https://proceedings.neurips.cc/paper/2021/hash/20aee3a5f4643755a79ee5f6a73050ac-Abstract.html`.

[26] Jiwei Li, Will Monroe, Alan Ritter, Dan Jurafsky, Michel Galley, and Jianfeng Gao. Deep reinforcement learning for dialogue generation. In Jian Su, Xavier Carreras, and Kevin Duh, editors, *Proceedings of the 2016 Conference on Empirical Methods in Natural Language Processing, EMNLP 2016, Austin, Texas, USA, November 1-4, 2016*, pages 1192–1202. The Association for Computational Linguistics, 2016. doi: 10.18653/v1/d16-1127. URL `https://doi.org/10.18653/v1/d16-1127`.

[27] Tianyi Lin, Chi Jin, and Michael I. Jordan. On gradient descent ascent for nonconvex-concave minimax problems. In *Proceedings of the 37th International Conference on Machine Learning, ICML 2020, 13-18 July 2020, Virtual Event*, volume 119 of *Proceedings of Machine Learning Research*, pages 6083–6093. PMLR, 2020. URL `http://proceedings.mlr.press/v119/lin20a.html`.

[28] Hao Liu and Pieter Abbeel. Behavior from the void: Unsupervised active pre-training. *Advances in Neural Information Processing Systems*, 34:18459–18473, 2021.

[29] Iou-Jen Liu, Unnat Jain, Raymond A. Yeh, and Alexander G. Schwing. Cooperative exploration for multi-agent deep reinforcement learning. In Marina Meila and Tong Zhang, editors, *Proceedings of the 38th International Conference on Machine Learning, ICML 2021, 18-24 July 2021, Virtual Event*, volume 139 of *Proceedings of Machine Learning Research*, pages 6826–6836. PMLR, 2021. URL `http://proceedings.mlr.press/v139/liu21j.html`.

[30] Siqi Liu, Guy Lever, Josh Merel, Saran Tunyasuvunakool, Nicolas Heess, and Thore Graepel. Emergent coordination through competition. In *7th International Conference on Learning Representations, ICLR 2019, New Orleans, LA, USA, May 6-9, 2019*. OpenReview.net, 2019. URL `https://openreview.net/forum?id=BkG8sjR5Km`.

[31] Siqi Liu, Guy Lever, Zhe Wang, Josh Merel, S. M. Ali Eslami, Daniel Hennes, Wojciech M. Czarnecki, Yuval Tassa, Shayegan Omidshafiei, Abbas Abdolmaleki, Noah Y. Siegel, Leonard Hasenclever, Luke Marris, Saran Tunyasuvunakool, H. Francis Song, Markus Wulfmeier, Paul Muller, Tuomas Haarnoja, Brendan D. Tracey, Karl Tuyls, Thore Graepel, and Nicolas Heess. From motor control to team play in simulated humanoid football. *Sci. Robotics*, 7(69), 2022. doi: 10.1126/scirobotics.abo0235. URL `https://doi.org/10.1126/scirobotics.abo0235`.

[32] Xiangyu Liu, Hangtian Jia, Ying Wen, Yujing Hu, Yingfeng Chen, Changjie Fan, Zhipeng Hu, and Yaodong Yang. Towards unifying behavioral and response diversity for open-ended learning in zero-sum games. In Marc'Aurelio Ranzato, Alina Beygelzimer, Yann N. Dauphin, Percy Liang, and Jennifer Wortman Vaughan, editors, *Advances in Neural Information Processing Systems 34: Annual Conference on Neural Information Processing Systems 2021, NeurIPS 2021, December 6-14, 2021, virtual*, pages 941–952, 2021. URL `https://proceedings.neurips.cc/paper/2021/hash/07bba581a2dd8d098a3be0f683560643-Abstract.html`.

[33] Qian Long, Zihan Zhou, Abhinav Gupta, Fei Fang, Yi Wu, and Xiaolong Wang. Evolutionary population curriculum for scaling multi-agent reinforcement learning. In *International Conference on Learning Representations*, 2020.

[34] Andrei Lupu, Hengyuan Hu, and Jakob N. Foerster. Trajectory diversity for zero-shot coordination. In Frank Dignum, Alessio Lomuscio, Ulle Endriss, and Ann Nowé, editors, *AAMAS '21: 20th International Conference on Autonomous Agents and Multiagent Systems, Virtual Event, United Kingdom, May 3-7, 2021*, pages 1593–1595. ACM, 2021. doi: 10.5555/3463952.3464170. URL `https://www.ifaamas.org/Proceedings/aamas2021/pdfs/p1593.pdf`.

[35] Pingchuan Ma, Tao Du, and Wojciech Matusik. Efficient continuous pareto exploration in multi-task learning. In *Proceedings of the 37th International Conference on Machine Learning, ICML 2020, 13-18 July 2020, Virtual Event*, volume 119 of *Proceedings of Machine Learning Research*, pages 6522–6531. PMLR, 2020. URL `http://proceedings.mlr.press/v119/ma20a.html`.

[36] Tengyu Ma. Why Do Local Methods Solve Nonconvex Problems?, March 2021. URL `http://arxiv.org/abs/2103.13462`. arXiv:2103.13462 [cs, math, stat].

[37] Marlos C. Machado, Marc G. Bellemare, and Michael Bowling. Count-based exploration with the successor representation. In *The Thirty-Fourth AAAI Conference on Artificial Intelligence, AAAI 2020, The Thirty-Second Innovative Applications of Artificial Intelligence Conference, IAAI 2020, The Tenth AAAI Symposium on Educational Advances in Artificial Intelligence, EAAI 2020, New York, NY, USA, February 7-12, 2020*, pages 5125–5133. AAAI Press, 2020. URL `https://ojs.aaai.org/index.php/AAAI/article/view/5955`.

[38] Viktor Makoviychuk, Lukasz Wawrzyniak, Yunrong Guo, Michelle Lu, Kier Storey, Miles Macklin, David Hoeller, Nikita Rudin, Arthur Allshire, Ankur Handa, and Gavriel State. Isaac gym: High performance gpu-based physics simulation for robot learning, 2021.

[39] Muhammad A. Masood and Finale Doshi-Velez. Diversity-inducing policy gradient: Using maximum mean discrepancy to find a set of diverse policies. In Sarit Kraus, editor, *Proceedings of the Twenty-Eighth International Joint Conference on Artificial Intelligence, IJCAI 2019, Macao, China, August 10-16, 2019*, pages 5923–5929. ijcai.org, 2019. doi: 10.24963/ijcai.2019/821. URL `https://doi.org/10.24963/ijcai.2019/821`.

[40] B.L. Miller and M.J. Shaw. Genetic algorithms with dynamic niche sharing for multimodal function optimization. In *Proceedings of IEEE International Conference on Evolutionary Computation*, pages 786–791, Nagoya, Japan, 1996. IEEE. ISBN 978-0-7803-2902-7. doi: 10.1109/ICEC.1996.542701. URL `http://ieeexplore.ieee.org/document/542701/`.

[41] Jean-Baptiste Mouret and Jeff Clune. Illuminating search spaces by mapping elites. *CoRR*, abs/1504.04909, 2015. URL `http://arxiv.org/abs/1504.04909`.

[42] Andrew Y Ng, Daishi Harada, and Stuart Russell. Policy invariance under reward transformations: Theory and application to reward shaping. In *Icml*, volume 99, pages 278–287, 1999.

[43] Olle Nilsson and Antoine Cully. Policy gradient assisted MAP-Elites. In *Proceedings of the Genetic and Evolutionary Computation Conference*, pages 866–875, Lille France, June 2021. ACM. ISBN 978-1-4503-8350-9. doi: 10.1145/3449639.3459304. URL `https://dl.acm.org/doi/10.1145/3449639.3459304`.

[44] Shayegan Omidshafiei, Karl Tuyls, Wojciech M Czarnecki, Francisco C Santos, Mark Rowland, Jerome Connor, Daniel Hennes, Paul Muller, Julien Pérolat, Bart De Vylder, et al. Navigating the landscape of multiplayer games. *Nature communications*, 11(1):1–17, 2020.

[45] Takayuki Osa, Voot Tangkaratt, and Masashi Sugiyama. Discovering diverse solutions in deep reinforcement learning by maximizing state-action-based mutual information. *Neural Networks*, 152:90–104, 2022. doi: 10.1016/j.neunet.2022.04.009. URL `https://doi.org/10.1016/j.neunet.2022.04.009`.

[46] Aldo Pacchiano, Jack Parker-Holder, Yunhao Tang, Krzysztof Choromanski, Anna Choromanska, and Michael Jordan. Learning to score behaviors for guided policy optimization. In *International Conference on Machine Learning*, pages 7445–7454. PMLR, 2020.

[47] Jack Parker-Holder, Luke Metz, Cinjon Resnick, Hengyuan Hu, Adam Lerer, Alistair Letcher, Alexander Peysakhovich, Aldo Pacchiano, and Jakob N. Foerster. Ridge rider: Finding diverse solutions by following eigenvectors of the hessian. In Hugo Larochelle, Marc'Aurelio Ranzato, Raia Hadsell, Maria-Florina Balcan, and Hsuan-Tien Lin, editors, *Advances in Neural Information Processing Systems 33: Annual Conference on Neural Information Processing Systems 2020, NeurIPS 2020, December 6-12, 2020, virtual*, 2020. URL `https://proceedings.neurips.cc/paper/2020/hash/08425b881bcde94a383cd258cea331be-Abstract.html`.

[48] Jack Parker-Holder, Aldo Pacchiano, Krzysztof Marcin Choromanski, and Stephen J. Roberts. Effective diversity in population based reinforcement learning. In Hugo Larochelle, Marc'Aurelio Ranzato, Raia Hadsell, Maria-Florina Balcan, and Hsuan-Tien Lin, editors, *Advances in Neural Information Processing Systems 33: Annual Conference on Neural Information Processing Systems 2020, NeurIPS 2020, December 6-12, 2020, virtual*, 2020. URL `https://proceedings.neurips.cc/paper/2020/hash/d1dc3a8270a6f9394f88847d7f0050cf-Abstract.html`.

[49] Alexander Peysakhovich and Adam Lerer. Consequentialist conditional cooperation in social dilemmas with imperfect information. In *6th International Conference on Learning Representations, ICLR 2018, Vancouver, BC, Canada, April 30 - May 3, 2018, Conference Track Proceedings*. OpenReview.net, 2018. URL `https://openreview.net/forum?id=BkabRiQpb`.

[50] Thomas Pierrot, Valentin Macé, Félix Chalumeau, Arthur Flajolet, Geoffrey Cideron, Karim Beguir, Antoine Cully, Olivier Sigaud, and Nicolas Perrin-Gilbert. Diversity Policy Gradient for Sample Efficient Quality-Diversity Optimization. In *Proceedings of the Genetic and Evolutionary Computation Conference*, pages 1075–1083, July 2022. doi: 10.1145/3512290.3528845. URL `http://arxiv.org/abs/2006.08505`. arXiv:2006.08505 [cs].

[51] Justin K. Pugh, Lisa B. Soros, and Kenneth O. Stanley. Quality Diversity: A New Frontier for Evolutionary Computation. *Frontiers in Robotics and AI*, 3, July 2016. ISSN 2296-9144. doi: 10.3389/frobt.2016.00040. URL `http://journal.frontiersin.org/Article/10.3389/frobt.2016.00040/abstract`.

[52] Tim Roughgarden, editor. *Beyond the Worst-Case Analysis of Algorithms*. Cambridge University Press, 2020. ISBN 9781108637435. doi: 10.1017/9781108637435. URL `https://doi.org/10.1017/9781108637435`.

[53] Mikayel Samvelyan, Tabish Rashid, Christian Schröder de Witt, Gregory Farquhar, Nantas Nardelli, Tim G. J. Rudner, Chia-Man Hung, Philip H. S. Torr, Jakob N. Foerster, and Shimon Whiteson. The starcraft multi-agent challenge. In Edith Elkind, Manuela Veloso, Noa Agmon, and Matthew E. Taylor, editors, *Proceedings of the 18th International Conference on Autonomous Agents and MultiAgent Systems, AAMAS '19, Montreal, QC, Canada, May 13-17, 2019*, pages 2186–2188. International Foundation for Autonomous Agents and Multiagent Systems, 2019. URL `http://dl.acm.org/citation.cfm?id=3332052`.

[54] Matthijs TJ Spaan. Partially observable markov decision processes. In *Reinforcement Learning*, pages 387–414. Springer, 2012.

[55] Hao Sun, Zhenghao Peng, Bo Dai, Jian Guo, Dahua Lin, and Bolei Zhou. Novel policy seeking with constrained optimization. *arXiv preprint arXiv:2005.10696*, 2020.

[56] Zhenggang Tang, Chao Yu, Boyuan Chen, Huazhe Xu, Xiaolong Wang, Fei Fang, Simon Shaolei Du, Yu Wang, and Yi Wu. Discovering diverse multi-agent strategic behavior via reward randomization. In *9th International Conference on Learning Representations, ICLR 2021, Virtual Event, Austria, May 3-7, 2021*. OpenReview.net, 2021. URL `https://openreview.net/forum?id=lvRTC669EY_`.

[57] Luca Venturi, Afonso S. Bandeira, and Joan Bruna. Neural networks with finite intrinsic dimension have no spurious valleys. *CoRR*, abs/1802.06384, 2018. URL `http://arxiv.org/abs/1802.06384`.

[58] Cédric Villani. *Optimal transport: old and new*, volume 338. Springer, 2009.

[59] Oriol Vinyals, Igor Babuschkin, Wojciech M. Czarnecki, Michaël Mathieu, Andrew Dudzik, Junyoung Chung, David H. Choi, Richard Powell, Timo Ewalds, Petko Georgiev, Junhyuk Oh, Dan Horgan, Manuel Kroiss, Ivo Danihelka, Aja Huang, Laurent Sifre, Trevor Cai, John P. Agapiou, Max Jaderberg, Alexander S. Vezhnevets, Rémi Leblond, Tobias Pohlen, Valentin Dalibard, David Budden, Yury Sulsky, James Molloy, Tom L. Paine, Caglar Gulcehre, Ziyu Wang, Tobias Pfaff, Yuhuai Wu, Roman Ring, Dani Yogatama, Dario Wünsch, Katrina McKinney, Oliver Smith, Tom Schaul, Timothy Lillicrap, Koray Kavukcuoglu, Demis Hassabis, Chris Apps, and David Silver. Grandmaster level in StarCraft II using multi-agent reinforcement learning. *Nature*, 575(7782):350–354, November 2019. ISSN 0028-0836, 1476-4687. doi: 10.1038/s41586-019-1724-z. URL `http://www.nature.com/articles/s41586-019-1724-z`.

[60] Rui Wang, Joel Lehman, Jeff Clune, and Kenneth O Stanley. Poet: open-ended coevolution of environments and their optimized solutions. In *Proceedings of the Genetic and Evolutionary Computation Conference*, pages 142–151, 2019.

[61] Tonghan Wang, Tarun Gupta, Anuj Mahajan, Bei Peng, Shimon Whiteson, and Chongjie Zhang. RODE: learning roles to decompose multi-agent tasks. In *9th International Conference on Learning Representations, ICLR 2021, Virtual Event, Austria, May 3-7, 2021*. OpenReview.net, 2021. URL `https://openreview.net/forum?id=TTUVg6vkNjK`.

[62] Shuang Wu, Jian Yao, Haobo Fu, Ye Tian, Chao Qian, Yaodong Yang, QIANG FU, and Yang Wei. Quality-similar diversity via population based reinforcement learning. In *The Eleventh International Conference on Learning Representations*, 2023.

[63] Yifan Wu, George Tucker, and Ofir Nachum. The laplacian in RL: learning representations with efficient approximations. In *7th International Conference on Learning Representations, ICLR 2019, New Orleans, LA, USA, May 6-9, 2019*. OpenReview.net, 2019. URL `https://openreview.net/forum?id=HJlNpoA5YQ`.

[64] Chao Yu, Akash Velu, Eugene Vinitsky, Yu Wang, Alexandre Bayen, and Yi Wu. The surprising effectiveness of ppo in cooperative, multi-agent games. *arXiv preprint arXiv:2103.01955*, 2021.

[65] Tom Zahavy, Brendan O'Donoghue, Andre Barreto, Volodymyr Mnih, Sebastian Flennerhag, and Satinder Singh. Discovering diverse nearly optimal policies with successor features. *arXiv preprint arXiv:2106.00669*, 2021.

[66] Tom Zahavy, Yannick Schroecker, Feryal M. P. Behbahani, Kate Baumli, Sebastian Flennerhag, Shaobo Hou, and Satinder Singh. Discovering policies with domino: Diversity optimization maintaining near optimality. *CoRR*, abs/2205.13521, 2022. doi: 10.48550/arXiv.2205.13521. URL `https://doi.org/10.48550/arXiv.2205.13521`.

[67] Yunbo Zhang, Wenhao Yu, and Greg Turk. Learning novel policies for tasks. In *International Conference on Machine Learning*, pages 7483–7492. PMLR, 2019.

[68] Rui Zhao, Jinming Song, Hu Haifeng, Yang Gao, Yi Wu, Zhongqian Sun, and Yang Wei. Maximum entropy population based training for zero-shot human-ai coordination. *arXiv preprint arXiv:2112.11701*, 2021.

[69] Zihan Zhou, Wei Fu, Bingliang Zhang, and Yi Wu. Continuously discovering novel strategies via reward-switching policy optimization. In *The Tenth International Conference on Learning Representations, ICLR 2022, Virtual Event, April 25-29, 2022*. OpenReview.net, 2022. URL `https://openreview.net/forum?id=hcQHRHKfN_`.

A Project Website

Check `https://sites.google.com/view/diversity-sipo` for GIF demonstrations.

B Additional Results

B.1 More Qualitative Results

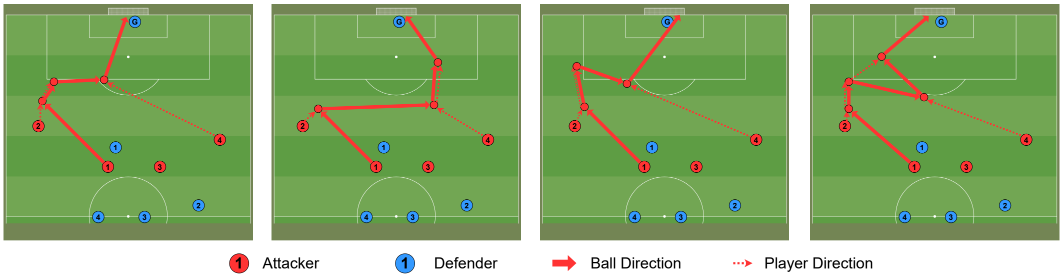

Figure 7: Visualization of learned behaviors in GRF *CA* across a single training trial.

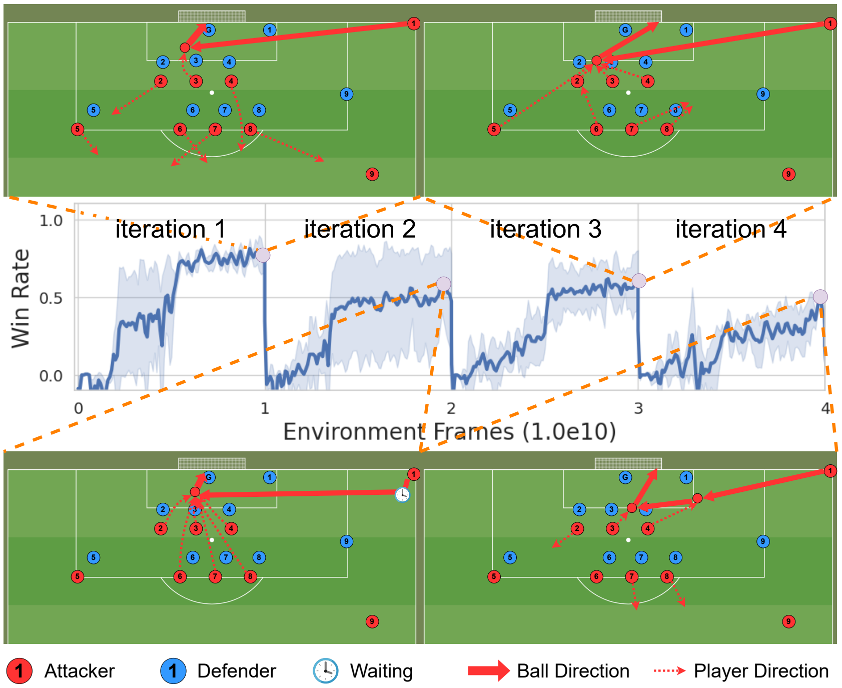

Figure 8: Visualization of learned behaviors in GRF *corner*.

We show additional visualization results in Fig. 7, Fig. 8, and Fig. 9. Corresponding GIF visualizations can be found in our project website.

B.2 Evaluation Metric and Protocol

B.2.1 Humanoid

The Humanoid locomotion task is well-studied in the Quality-Diversity (QD) community, enabling the application of well-defined behavior descriptors (BD) to assess diversity scores. While domain-agnostic metrics like DvD scores can also be applied, we consider domain-specific BDs to be more appropriate and accurate for evaluation in this setting.

Table 7: k-nearest neighbor state entropy estimation in GRF. Population size $M = 4$.

	ours		baselines				
	SIPO-RBF	SIPO-WD	DIPG	SMERL[1]	DvD[2]	RSPO[1]	PG (random seeding)
3v1	0.009(0.000)	0.012(0.000)	0.010(0.001)	0.011(0.002)	0.010(0.000)	0.011(0.001)	0.009(0.001)
CA	0.037(0.000)	0.031(0.006)	0.036(0.002)	-	-	0.034(0.001)	0.039(0.001)
Corner	0.028(0.001)	0.031(0.001)	0.030(0.002)	-	-	-	0.028(0.002)

[1] The learned policy in some iteration cannot even collect a single winning trajectory. We are unable to compute diversity score.

[2] Training DvD in *CA* and *corner* requires >24GB GPU memory, which exceeds our memory limit.

B.2.2 SMAC

Complex multi-agent tasks like SMAC lack well-defined BDs. Hence, domain-agnostic diversity measures such as the state-entropy measure should be applied. Moreover, different SMAC winning strategies tend to visit different areas of the map, which can be usually captured by the state-entropy measure.

B.2.3 GRF

In our initial study of the GRF task, diversity was evaluated using the k-nearest-neighbor state entropy estimation as in SMAC (see Table 7). However, we observed a significant difference between the computed scores and visualized behaviors. Further investigation revealed that state entropy can sometimes report fake diversity in GRF. For example, the ball-moving route is highly fine-grained between nearby players in the counter-attack (CA) scenario, and additional passes may not change the state entropy significantly. Instead, agents' positions play a crucial role in this scenario, where different shooting positions can introduce substantial state variance and lead to a higher entropy score. As an example, readers can refer to the replays of SIPO-RBF (4 iterations of seed 2) and PG (seed 2, 1002, 2002, and 3002), where SIPO-RBF discovers four distinct passing strategies, while PG keeps passing the ball to the same player. Nevertheless, the state entropy of PG (0.0397) is higher than that of SIPO-RBF (0.0378).

Hence, we counted the number of distinct policies according to their ball-passing routes, such as passing the ball to different players or shooting with different players, to evaluate diversity in GRF. To quantify these differences, we extracted the positions of the ball and the players in the field and calculated the nearest ally player ID to the ball across a winning episode. We then removed timesteps where the nearest distance was above a pre-defined threshold of 0.03. Typically, these timesteps correspond to instances when the ball is being transferred among players, making the nearest player ID irrelevant. Next, we removed consecutive duplicate player IDs from the resulting sequence to obtain a concise and informative embedding of the ball passing route. By comparing the lengths of their respective embeddings and verifying that the player IDs in each embedding are identical, we determined whether two policies exhibit similar behavior.

We acknowledge that existing diversity measures may not be applicable in GRF, and hence we opted for this novel approach to evaluate diversity. Additionally, we experimented with using raw

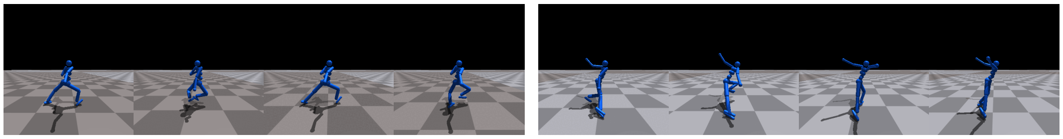

Iteration 1 Iteration 3

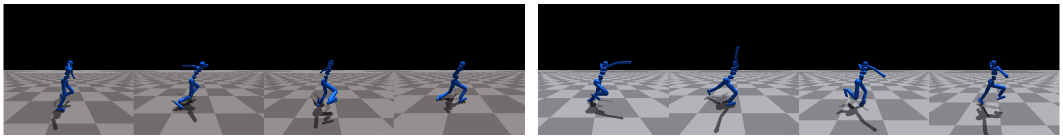

Iteration 2 Iteration 4

Figure 9: Visualization of learned behaviors in Humanoid.

observations, which include ball ownership information provided by the game engine, but found it to be highly inaccurate based on our visualization.

B.3 Ablation Study of the State Input

B.3.1 Vectorized States in Google Research Football

We perform an additional ablation study over the input of our diversity measure in GRF *3v1* scenario with SIPO-WD. We consider the following kinds of state input besides the default state input we adopted in Sec. 6:

- full observation (named *full*, 115 dims);
- default state input with random noises of the same dimension (named *random*, 36 dims).

The numbers of visually distinct strategies are listed in Table 8. The performance of *full* and *random* is similarly good. The result implies that the learnable discriminator can automatically filter out irrelevant states to some extent, and that SIPO-WD performs relatively robust w.r.t. different state input of the diversity measure.

Table 8: State input ablation. The table shows the number of distinct strategies in GRF *3v1*.

	SIPO-WD	full	random
3v1	3.0 (0.0)	3.0 (0.8)	3.0 (0.0)

B.3.2 RGB Images in Locomotion Tasks

We run SIPO-WD in the visual Humanoid task based on Isaac Gym [38]. The training protocol is similar to the state-only version (i.e., the input of policy and intrinsic rewards are both locomotion states of the Humanoid) except that we stack recent 4 RGB camera observations (84×84) as the input of intrinsic rewards in Eq. 9. We adopt the training code developed in Isaac Gym and the default PPO configuration. The backbone of the discriminator is composed of 4 convolutional layers with kernel size 3, stride 2, padding 1, and [16, 32, 32, 32] channels. Then the feature is passed to an MLP with 1 hidden layer and 256 hidden units. The activation function is leaky ReLU with slope 0.2.

We also compute the pairwise distance of joint torques as in the state-only version and show the result in Table 9. Visualizations are shown in Fig. 10. SIPO-WD can also learn meaningful diverse behaviors with RGB images as the state input thanks to the learnable Wasserstein discriminator. This implies that our algorithm can be naturally extended to high-dimensional states and incorporated with advances in representation learning, which may be a potential future direction.

B.4 How to Adjust Constraint-Related Hyperparameters

Three hyperparameters are essential in the implementation of the intrinsic reward r_{int}: the threshold δ, the intrinsic reward scale factor α, and the variance factor σ in $r_{\text{int}}^{\text{RBF}}$. These parameters differ under

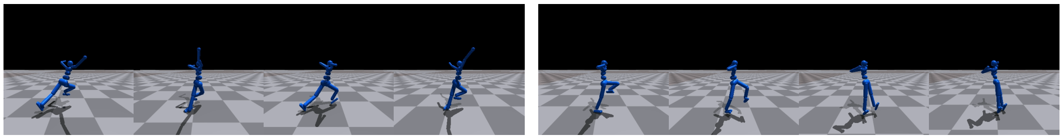

(a) normal running

(b) left-leg jumping

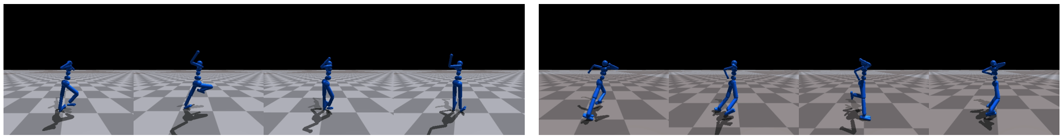

(c) right-leg jumping

(d) hand-balanced mincing

Figure 10: Results of SIPO-WD in the visual Humanoid task.

Table 9: Pairwise distance of joint torques (i.e., diversity score) in Humanoid with visual input. Results in visual experiments are averaged over 3 seeds.

SIPO-WD (visual)	SIPO-WD	RSPO (best baseline)
0.62 (0.26)	0.71 (0.23)	0.53 (0.05)

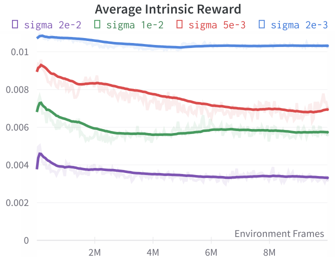

Figure 11: Average intrinsic reward during training π_1.

Table 10: The values of δ and α in different environments.

	football			smac	
	3v1	*corner*	*CA*	2m_vs_1z	2c_vs_64zg
δ^{WD}	0.004	0.01	0.012	0.02	0.2
α^{WD}	1	1	0.5	0.5	0.05
δ^{RBF}	0.03	0.01	0.015	0.002	0.001
α^{RBF}	0.001	0.001	0.001	0.001	0.001
σ^2	0.02	0.02	0.02	0.02	0.02

different domains and must be adjusted individually. We find proper parameters by running two iterations without constraints and get two similar policies π_0 and π_1. We record r_{int} during training π_1 and the trend is shown in Fig. 11. Not surprisingly, r_{int} gradually decreases as training proceeds.

Threshold We set $\delta = c_1 D_{\mathcal{S}}(\pi_0, \pi_1)$. We try several different $c_1 \in \{1, 1.2, 1.4, 1.6, 1.8, 2.0\}$ and find that $c_1 = 1.2$ or 1.4 are universal proper solutions for all the experimental environments.

Intrinsic Scale Factor We need to balance the intrinsic reward r_{int} and the original reward J so that neither of the two rewards can dominate the training process. Empirically, the maximums of the two rewards should be in the same order of magnitude. i.e., $\max_\pi J(\pi) = \alpha \times c_2 \lambda_{max} \delta$, where $c_2 = O(1)$. When c_2 is too large, the new-trained policy π_j will oscillate near the boundary of $D(\pi_i, \pi_j) = \delta$ for some pre-trained policy p_i. Conversely, when c_2 is too small, the intrinsic reward r_{int} cannot yield diverse strategies. In experiments, we set $c_2 = 1.0$.

Variance Factor We sweep the variance factor across $\{1e-3, 5e-3, 1e-2, 2e-2, 1e-3\}$ by training π_1 and observe the trend of intrinsic rewards. We find the steepest trend and select the corresponding σ. Empirically, we find that our algorithm performs robustly well when $\sigma^2 = 0.02$.

The δ and α of GRF and SMAC are listed in Table 10.

B.5 Task Performance Evaluation

The evaluation win rates of the demonstrated visualization results in SMAC and GRF are shown in Table 11. Evaluated episode returns in Humanoid are shown in Table 12.

Table 11: Evaluation win rate (%) of the demonstrated visualization results in SMAC and GRF.

	SMAC		GRF		
	2m1z	*2c64zg*	*3v1*	*CA*	*corner*
π_1	100.0(0.0)	98.1(2.1)	92.3(6.2)	48.2(10.4)	78.2(16.2)
π_2	99.6(0.9)	100.0(0.0)	82.1(8.4)	43.8(42.2)	57.0(37.7)
π_3	100.0(0.0)	96.9(3.3)	90.7(1.1)	54.7(30.6)	55.7(20.8)
π_4	99.6(0.6)	98.6(2.4)	63.6(45.0)	17.2(30.0)	30.7(29.0)
π_5	-	-	85.4(9.1)	-	-
π_6	-	-	93.2(1.9)	-	-
π_7	-	-	64.6(32.5)	-	-

Table 12: Episode returns in Humanoid.

	SIPO-RBF	SIPO-WD	SIPO-WD (visual)
π_1	4863.9(970.3)	3909.4(533.4)	4761.3(107.8)
π_2	3746.5(488.0)	3784.2(481.2)	4349.3(169.0)
π_3	3092.0(805.0)	3770.4(674.4)	4724.3(946.5)
π_4	2332.8(519.8)	3589.6(387.4)	3819.7(588.7)

B.6 Computation of Action-Based Measures in the Grid-World Example

We consider the policies illustrated in Fig. 12. These policies are all optimal since these actions only include "right" and "down" and actions on non-visited states can be arbitrary. We only mark actions on states visited by any of these 3 policies and actions on other states can be considered the same.

B.6.1 Action-Distribution-Based Measures

Action-distribution-based diversity measures can be defined as

$$D_{\mathcal{A}}(\pi_i, \pi_j) = \mathbb{E}_{s\sim q(s)}\left[\tilde{D}\left(\pi_i(\cdot \mid s) \| \pi_j(\cdot \mid s)\right)\right], \tag{10}$$

where $\tilde{D}(\cdot,\cdot) : \triangle \times \triangle \to \mathbb{R}$ is a measure over action distributions and $q : \triangle(\mathcal{S})$ is a state distribution. Here, we consider q to be the joint state distribution visited by π_i and π_j.

KL Divergence KL divergence is defined by

$$D_{\text{KL}}\left(\pi_i(\cdot \mid s), \pi_j(\cdot \mid s)\right) = \int_{\mathcal{A}} \pi_i(a \mid s) \log \frac{\pi_i(a \mid s)}{\pi_j(a \mid s)} \mathrm{d}a.$$

When $\pi_j(a \mid s) = 0$ at any state s, KL divergence is $+\infty$. Since the trajectories of these policies have disjoint states, $D^{\text{KL}}_{\mathcal{A}}(\pi_1, \pi_2) = D^{\text{KL}}_{\mathcal{A}}(\pi_1, \pi_3) = +\infty$. Similar results can be obtained for cross-entropy.

JSD$_\gamma$ JSD$_\gamma$ was defined in [34] and we consider two special cases when $\gamma = 0$ and $\gamma = 1$.

As illustrated by [34], JSD$_0$ measures the expected number of times two policies will "disagree" by selecting different actions. On trajectories induced by π_1 and π_2, there are $4 + 4$ states that π_1 disagrees with π_2 (π_1 and π_2 are symmetric) and $D^{\text{JSD}_0}_{\mathcal{A}}(\pi_1, \pi_2) = 8/16 = 1/2$. Similarly, π_1 and π_3 only disagree at the initial state, therefore we have $D^{\text{JSD}_0}_{\mathcal{A}}(\pi_1, \pi_3) = 2/16 = 1/8$.

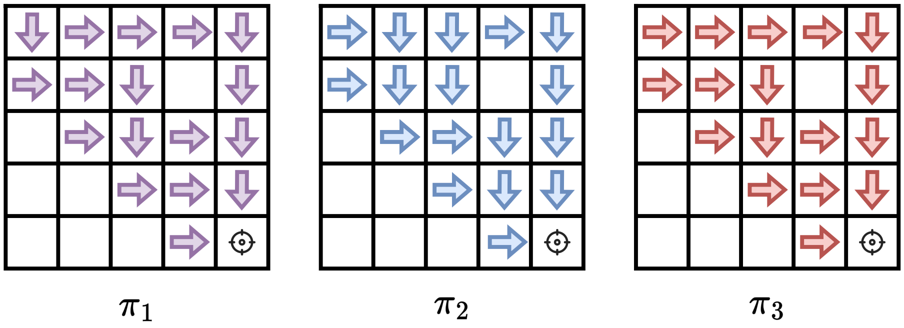

Figure 12: Policies in the grid-world example when $N_G = 5$.

JSD_1 is defined by

$$\begin{aligned}\text{JSD}_1(\pi_i, \pi_j) = & -\frac{1}{2}\sum_{\tau_i} P(\tau_i \mid \pi_i) \sum_{t=1}^{T} \frac{1}{T} \log \frac{\pi_i(\tau_i) + \pi_j(\tau_i)}{2\pi_i(\tau_i)} \\ & -\frac{1}{2}\sum_{\tau_j} P(\tau_j \mid \pi_j) \sum_{t=1}^{T} \frac{1}{T} \log \frac{\pi_i(\tau_j) + \pi_j(\tau_j)}{2\pi_j(\tau_j)}.\end{aligned}$$

Since each of the policies considered only induces a single trajectory and $\pi_i(\tau_j) = 0\ (i \neq j)$, we can easily compute

$$D_{\mathcal{A}}^{\text{JSD}_1}(\pi_1, \pi_2) = D_{\mathcal{A}}^{\text{JSD}_1}(\pi_1, \pi_3) = \log 2$$

Wasserstein Distance Wasserstein distance or Earth Moving Distance (EMD) is 1 if two policies disagree on a state and 0 otherwise. Therefore, it equals to $D_{\mathcal{A}}^{\text{JSD}_0}$.

B.6.2 Action Norm

We embed the action "right" as vector $[1, 0]$ since it increases the x-coordinate by 1 and the action "down" as vector $[0, -1]$ since it decreases the y-coordinate by 1. This embedding can be naturally extended to a continuous action space with velocity actions. Following [48], we compute the action norm over a uniform distribution on states. We can see that there are 7 states where π_1 and π_2 perform differently and 1 state (the initial state) where π_1 and π_3 perform differently. Therefore, we can get $D(\pi_1, \pi_2) = \sqrt{7}$ and $D(\pi_1, \pi_3) = 1$.

B.6.3 State-Distance-Based Measures

State L_2 Norm Similar to action L_2 norm, we concatenate the coordinates instead of actions as the embedding and compute the L_2 norm between embedding.

Wasserstein Distance Wasserstein distance is tractable in the grid-world example. We consider 7 states (except the initial and final states) in each trajectory and compute the pair-wise distance as matrix C. Then we solve the following linear programming

$$\begin{aligned}\min_{\gamma} \quad & \sum_{i,j} \gamma \odot C \\ \text{s.t.} \quad & \gamma \mathbf{1} = a,\ \gamma^T \mathbf{1} = b \\ & \gamma_{i,j} \geq 0\end{aligned}$$

where $\odot$ means element-wise multiplication, $\mathbf{1}$ is a all-one vector, $a = [\mathbf{1}^T, \mathbf{0}^T]^T$ and $b = [\mathbf{0}^T, \mathbf{1}^T]^T$ is the marginal state distribution of each policy.

C Environment Details

C.1 Details of the 2D Navigation Environment

The navigation environment has an agent circle with size a and 4 landmark circles with size b. We pre-specify a threshold c and constrain that the distance of final states reaching different landmarks must be larger than c. Correspondingly, landmark circles are randomly initialized by constraining the pairwise distance between centers to be larger than a threshold $c + 2(a + b)$ such that the final-state constraint is valid. An episode ends if the agent touches any landmarks, i.e., the distance between the center of the agent and the center of the landmark $d < a + b$, or 1000 timesteps have elapsed. The observation space includes the positions of the agent and all landmarks, which is a 10-dimensional vector. The action space is a 2-dimensional vector, which is the agent velocity. The time interval is set to be $\Delta t = 0.1$, i.e., the next position is computed by $x_{t+1} = x_t + \Delta t \cdot v$. The reward is 1 if the agent touches the landmark and 0 otherwise.

Table 13: Hyperparameters in the 2D navigation environment.

discount	GAE λ	PPO epochs	clip parameter	entropy bonus	$\lambda_{\max}$	actor lr	critic lr	Lagrange lr	batch size
0.997	0.95	10	0.2	0	10	3e-4	1e-3	0.5	4000

C.2 Details of Environments

We provide training configurations and environment introductions below and refer readers to our project website in App. A for visualizations of these environments.

Humanoid We use the Humanoid environment in IsaacGym [38] with default observation and action spaces. The input of intrinsic rewards or diversity measure is the observation without all torque states.

SMAC We adopt the SMAC environment in the MAPPO codebase[1] with the same configuration as Yu et al. [64]. The input of intrinsic rewards or diversity measure is the state of all allies, including positions, health, etc.

On the “easy” map *2m_vs_1z*, two marines must be controlled to defeat a Zealot. The marines can attack from a distance, while the Zealot’s attacks are limited to close range. A successful strategy involves alternating the marines’ attacks to distract the Zealot. On the “hard” map *2c_vs_64zg*, two colossi must be controlled by the agents to fight against 64 zergs. The colossi have a wider attack range and can move over cliffs. Strategies on this map may include hit-and-run tactics, waiting in corners, or dividing and conquering enemies. The level of difficulty is determined by the learning performance of existing MARL algorithms. Harder maps require more exploration and training steps.

GRF We adopt the “simple115v2” representation as observation with both “scoring” and “checkpoint” reward. The reward is shared across all agents. The input of intrinsic rewards or diversity measure is the position and velocity of all attackers and the ball. All policies are trained to control the left team to score against build-in bots.

academy_3_vs_1_with_keeper: In this scenario, a team of three players (left) try to score a goal against a single defender and a goalkeeper. The left team starts with the ball and has to dribble past the defender and the goalkeeper to score a goal.

academy_counterattack_easy: In this scenario, the left team starts with the ball in the front-yard and try to score a goal against several defenders. All eleven players in the left players can be controlled.

academy_corner: In this scenario, the left team tries to score a goal from a corner kick. The right team defends the goal and tries to prevent the left team from scoring. All eleven players in the left players can be controlled.

D Implementation Details

D.1 2D Navigation

We apply PPO with Lagrange multipliers to optimize the policy and hyperparameters are summarized in Table 13. $D(\pi_i, \pi_j)$ is simply taken as the L_2 distance of the final state reached by π_i and π_j, i.e., $D(\pi_i, \pi_j) = \|s_H^{\pi_i} - s_H^{\pi_j}\|^2$. The applied algorithm is the same as SIPO (see Appendix G) except that the intrinsic reward is only computed at the last timestep.

D.2 SIPO

In the i-th iteration ($1 \le i \le M$), we learn an actor and a critic with i separate value heads to accurately predict different return terms, including $i-1$ intrinsic returns for the diversity constraints and the environment reward. We include all practical tricks mentioned in [64] because we find them all critical to algorithm performance. We use separate actor and critic networks, both with hidden size 64 and a GRU layer with hidden size 64. The common hyperparameters for SIPO,

---

[1] `https://github.com/marlbenchmark/on-policy`

Table 14: Common hyperparameters for SIPO, baselines, and ablations.

discount	GAE λ	actor lr	critic lr	clip parameter	entropy bonus	GRF batch size	SMAC batch size
0.99	0.95	5e-4	1e-3	0.2	0.01	9600	3200

Table 15: SIPO hyperparameters across all environments.

$\lambda_{\max}$	Discriminator lr	Lagrangian lr
10	4.0e-4	0.1

baselines, and ablations are listed in Table 14. Other environment-specific parameters, such as PPO epochs and mini-batch size, are all the same as [64]. Besides, Table 10 and Table 15 lists some extra hyperparameters for SIPO.

D.3 Baselines

We re-implement all baselines with PPO based on the MAPPO [64] project. All algorithms run for the same number of environment frames. Specific hyperparameters for baselines can be found in Appendix D.3.

SMERL SMERL trains a latent-conditioned policy that can robustly adapt to new scenarios. It promotes diversity by maximizing the mutual information between states and the latent variable. We implement SMERL with PPO, where the actor and the critic take as the input the concatenation of observation and a one-hot latent variable. The discriminator is a 2-layer feed-forward network with 64 hidden units. The learning rate of the discriminator is the same as the learning rate of the critic network. The input of the discriminator is the same as the input we use for SIPO-WD. The critic has 2 value heads for an accurate estimation of intrinsic return. Since SMERL trains a single latent-conditioned policy, we train SMERL for $M\times$ more environment steps, such that total environment frames are the same. The scaling factor of intrinsic rewards is 0.1 and the threshold for diversification is $[0.81, 0.45, 0.72]$ $(0.9 \times [0.9, 0.5, 0.8])$ for “3v1”, “counterattack”, and “corner” respectively.

DvD DvD simultaneously trains a population of policies to maximize the determinant of a kernel matrix based on action difference. We concatenate the one-hot actions along a trajectory as the behavioral embedding. The square of the variance factor, i.e., σ^2 in the RBF kernel, is set to be the length of behavioral embedding. We also use the same Bayesian bandits as proposed in the original paper. Training DvD in “counterattack” and “corner” exceeds the GPU memory and we exclude the results in the main body.

DIPG DIPG iteratively maximizes the maximum mean discrepancy (MMD) distance between the state distribution of the current policy and previously discovered policies. For DIPG, we follow the opensource implementation[2]. We set the same variance factor in the RBF kernel as SIPO-RBF and apply the same state as the input of the RBF kernel. We sweep the coefficient of MMD loss among $\{0.1, 0.5, 0.9\}$ and find 0.1 the most appropriate (larger value will cause training instability). We use the same method to save archived trajectories as SIPO and the input of the RBF kernel is the same as the input we use for SIPO-RBF. To improve training efficiency, we only back-propagate the MMD loss at the first PPO epoch.

RSPO RSPO iteratively discovers diverse policies by optimizing extrinsic rewards on novel trajectories while optimizing diversity on other trajectories. The diversity measure is defined as the action-cross entropy along the trajectory. For RSPO, we follow the opensource implementation[3] and use the same hyperparameters on the SMAC *2c_vs_64zg* map in the original paper for GRF experiments.

---

[2] `https://github.com/dtak/DIPG-public`

[3] `https://github.com/footoredo/rspo-iclr-2022`

TrajDi TrajDi was originally designed for cooperate multi-agent domains to facillitate zero-shot coordination. It defines a generalized Jensen-Shanon divergence objective between policy action distributions. Then this objective and rewards are simultaneously optimized via population-based training. We tried TrajDi in SMAC and GRF. We sweep the action discount factor among $\{0.1, 0.5, 0.9\}$ and the coefficient of TrajDi loss among $\{0.1, 0.01, 0.001\}$. However, TrajDi fails to converge in the "3v1" scenario and exceeds the GPU memory in the "counterattack" and "corner" scenarios. Therefore, we exclude the performance of TrajDi in the main body.

D.4 Ablation Study Details

For the three ablation studies: fix-L, CE, and filter, we list the specific hyperparameters here:

- fix-L: we set the Lagrange multiplier to be 0.2;
- CE: the threshold is 3.800 and the intrinsic reward scale factor is $1/1000$ of that in the WD setting;
- filter: all the hyperparameters in the setting is the same as those in the WD setting.

E Proofs

E.1 Proof of theorem 4.1

Theorem 4.1. *Assume D is a distance metric. Denote the optimal value of Problem 3 as T_1. Let $T_2 = \sum_{i=1}^{M} J(\tilde{\pi}_i)$ where*

$$\begin{aligned} \tilde{\pi}_i = \arg\max_{\pi_i} \quad & J(\pi_i) \\ \textit{s.t.} \quad & D(\pi_i, \tilde{\pi}_j) \geq \delta/2, \quad \forall 1 \leq j < i \end{aligned} \tag{3}$$

for $i = 1, \dots, M$, then $T_2 \geq T_1$.

Proof. Suppose the optimal solution of Problem 3 is $\pi_1, \pi_2, ..., \pi_M$ satisfying $J(\pi_1) \geq J(\pi_2) \geq ... \geq J(\pi_M)$ and the optimal solution of Problem 6 is $\tilde{\pi}_1, \tilde{\pi}_2, ..., \tilde{\pi}_M$ satisfying $J(\tilde{\pi}_1) \geq J(\tilde{\pi}_2) \geq ... \geq J(\tilde{\pi}_M)$.

Assume the contrary that Thm. 4.1 is not true, which means $\sum_{i=1}^{M} J(\pi_i) = T_1 > T_2 = \sum_{i=1}^{M} J(\tilde{\pi}_i)$. Then we choose the smallest number $N \leq M$ that satisfies

$$\sum_{i=1}^{N} J(\pi_i) > \sum_{i=1}^{N} J(\tilde{\pi}_i).$$

By $T_1 > T_2$ we know that N exists. In addition, because Problem 6 solves unconstrained RL in the first iteration, we know that $\tilde{\pi}_1 = \arg\max_\pi J(\pi)$ and then $J(\pi_1) \leq J(\tilde{\pi}_1)$. Therefore, $N \geq 2$.

Suppose $J(\pi_N) \leq J(\tilde{\pi}_N)$. Then we have

$$\sum_{i=1}^{N-1} J(\pi_i) > \sum_{i=1}^{N-1} J(\tilde{\pi}_i).$$

Contradicting the fact that N is the smallest number satisfies that equation.

Hence, we know that $J(\pi_N) > J(\tilde{\pi}_N)$. Then

$$J(\pi_1) \geq J(\pi_2) \geq ... \geq J(\pi_N) > J(\tilde{\pi}_N).$$

Consider the optimization problem of $\tilde{\pi}_N$:

$$\begin{aligned} \tilde{\pi}_N = \arg\max_{\pi} \quad & J(\pi) \\ \text{s.t.} \quad & D(\pi, \tilde{\pi}_j) \geq \delta/2, \quad \forall 1 \leq j < N. \end{aligned}$$

This optimization does not find $\{\pi_1, \ldots, \pi_N\}$ but find $\tilde{\pi}_N$, which means that for each π_i, $1 \le i \le N$, there exists $1 \le j_i < N$ such that $D(\pi_i, \tilde{\pi}_{j_i}) < \delta/2$. Otherwise, we will get the solution of the above problem as π_i instead of $\tilde{\pi}_N$.

By the Pigeonhole Principle, we know that there exist two indexes $i_1 \in [N]$ and $i_2 \in [N]$ $(i_1 \ne i_2)$ such that $j_{i_1} = j_{i_2} = \hat{j}$. Then we have

$$D(\pi_{i_1}, \pi_{i_2}) \le D(\pi_{i_1}, \tilde{\pi}_{\hat{j}}) + D(\pi_{i_2}, \tilde{\pi}_{\hat{j}}) < \delta/2 + \delta/2 = \delta,$$

where the inequality follows by the triangle inequality of the distance function.

It contradict with the fact that $D(\pi_{i_1}, \pi_{i_2}) \ge \delta$ in Problem 3.

Therefore, we prove the theorem $\sum_{i=1}^{M} J(\pi_i) = T_1 \le T_2 = \sum_{i=1}^{M} J(\tilde{\pi}_i)$. □

E.2 Proof of Theorem 5.1

In this section, we consider the i-th iteration of SIPO illustrated in Eq. (4). For the sake of simplicity, we use $a \le \boldsymbol{\lambda} \le b$ for vector $\boldsymbol{\lambda}$ to denote each component of $\boldsymbol{\lambda}$ satisfies $a \le \lambda_i \le b$, where $a, b \in \mathbb{R}$. We use π to denote the policy we are optimizing, and π_j $(1 \le j < i)$ to denote a previously obtained policy. We denote the Lagrange function as $L(\pi, \boldsymbol{\lambda}) = -J(\pi) - \sum_{j=1}^{i-1} \lambda_j \left(D(\pi, \pi_j) - \delta\right)$.

To prove Theorem 5.1, we consider the following two optimization problems:

$$(\pi_i, \boldsymbol{\lambda}^\star) = \arg\min_{\pi} \max_{\boldsymbol{\lambda} \ge 0} L(\pi, \boldsymbol{\lambda}) \tag{11}$$

and

$$(\tilde{\pi}_i, \tilde{\boldsymbol{\lambda}}^\star) = \arg\min_{\pi} \max_{0 \le \boldsymbol{\lambda} \le \Lambda} L(\pi, \boldsymbol{\lambda}), \tag{12}$$

where $\Lambda = \frac{1}{\epsilon_0}$ and $\epsilon_0 > 0$ is sufficiently small.

We make the following assumptions to prove this theorem:

Assumption E.1. $0 \le J(\cdot) \le 1$.

Assumption E.2. $\forall \boldsymbol{\lambda} \ge 0,\ L(\cdot, \boldsymbol{\lambda})$ is l-smooth and ζ-Lipschitz.

We may notice that, solving optimization problem (11) is hard because its domain is unbounded. Therefore, we make some approximation and consider bounded optimization problem (12). First we prove the following lemma about the value function J:

Lemma E.3. $J(\pi_i) \le J(\tilde{\pi}_i)$.

Proof. As the domain of $\boldsymbol{\lambda}$ in Eq. 12 is smaller than Eq. (11), we have $L(\pi_i, \boldsymbol{\lambda}) \ge L(\tilde{\pi}_i, \tilde{\boldsymbol{\lambda}})$.

By the fundamental property of Lagrange duality, we know that L achieves its optimal value when $\boldsymbol{\lambda} = 0$ and the optimal value is $-J(\pi_i)$.

By the optimality of $(\tilde{\pi}_i, \tilde{\boldsymbol{\lambda}}^\star)$, we know that

$$-\sum_{j=1}^{i-1} \tilde{\lambda}_j^\star (D(\tilde{\pi}_i, \pi_j) - \delta) \ge 0. \tag{13}$$

Then we have

$$-J(\pi_i) = L(\pi_i, \boldsymbol{\lambda}^\star) \ge \tilde{L}(\tilde{\pi}_i, \tilde{\boldsymbol{\lambda}}^\star) = -J(\tilde{\pi}_i) - \sum_{j=1}^{i-1} \tilde{\lambda}_j^\star (D(\tilde{\pi}_i, \pi_j) - \delta) \ge -J(\tilde{\pi}_i).$$

□

Then we prove the distance between optimal policy $\tilde{\pi}_i$ in problem (12) and optimal policy π_i in problem (11) is very small:

Lemma E.4. *Under Assumption E.1,* $D(\tilde{\pi}_i, \pi_j) \ge \delta - \epsilon_0,\ \forall 1 \le j < i.$

Proof. We prove by contradiction.

Suppose there exists $1 \le j_0 < i$, $D(\tilde{\pi}_i, \pi_{j_0}) < \delta - \epsilon_0$. Then we choose $\hat{\boldsymbol{\lambda}}$ such that

$$\hat{\lambda}_j = \begin{cases} \Lambda & j = j_0\,, \\ 0 & 1 \le j < i, j \ne j_0\,. \end{cases}$$

By the Assumption E.1, Eq. (13), and $\Lambda = \frac{1}{\epsilon_0}$, we have

$$0 \ge -J(\pi_i) = L(\pi_i, \boldsymbol{\lambda}^\star) \ge L(\tilde{\pi}_i, \tilde{\boldsymbol{\lambda}}^\star) \ge L(\tilde{\pi}_i, \hat{\boldsymbol{\lambda}}) \ge -1 - \Lambda(D(\tilde{\pi}_i, \pi_{j_0}) - \delta) > 0.$$

That is a contradiction. So we have proved that

$$D(\tilde{\pi}_i, \pi_j) \ge \delta - \epsilon_0, \quad \forall 1 \le j < i.$$

□

From the deduction above, we get the following approximation lemma:

Lemma E.5. *Denote the optimal solution of Eq. 11 and Eq. 12 as (π_i, λ) and $(\tilde{\pi}_i, \tilde{\lambda})$ respectively. Then we have the following approximation about the optimal value and distance:*

$$J(\pi_i) \le J(\tilde{\pi}_i)$$
$$D(\tilde{\pi}_i, \pi_j) \ge \delta - \epsilon_0, \quad \forall 1 \le j < i$$

Proof. This lemma follows directly by Lemma E.3 and Lemma E.4. □

Therefore, it is reasonable to consider the constrained optimization problem (12) instead of primal problem (11) because we have proved that the optimal value doesn't get smaller and the distance of policy is ϵ_0-approximation of the primal problem. Finally we use the conclusion in the paper [27] to analysis the convergence of problem (12):

Lemma E.6. *([27], Theorem 4.8) Under Assumption E.2, solving Eq. (12) via two-timescale GDA with learning rate $\eta_\pi = \Theta(\epsilon^4/l^3\zeta^2\Lambda^2)$ and $\eta_{\boldsymbol{\lambda}} = \Theta(1/l)$ requires*

$$\mathcal{O}\left(\frac{l^3\zeta^2\Lambda^2 C_1}{\epsilon^6} + \frac{l^3\Lambda^2 C_2}{\epsilon^4}\right)$$

iterations to converge to an ϵ-stationary point $\pi_i^\star$, where C_1 and C_2 are the constants that depend on the distance between the initial point and the optimal point.

Theorem 5.1. *Under assumptions E.1 and E.2 and learning rate with learning rate $\eta_\pi = \Theta(\epsilon^4/l^3\zeta^2\Lambda^2)$ and $\eta_{\boldsymbol{\lambda}} = \Theta(1/l)$, SIPO converges to an ϵ-stationary point with convergence rate $\mathcal{O}\left(\frac{l^3\zeta^2\Lambda^2 C_1}{\epsilon^6} + \frac{l^3\Lambda^2 C_2}{\epsilon^4}\right)$.*

Proof. We consider the following constraint nonconvex-concave optimization:

$$\min_{\pi} \max_{0 \le \boldsymbol{\lambda} \le \Lambda} L(\pi, \boldsymbol{\lambda})\,. \tag{14}$$

Following Lemma E.6, we know that the Two-Timescale GDA algorithm converges to an ϵ-stationary point π_i^*.

From the above deduction, the Two-Timescale GDA algorithm requires $\mathcal{O}\left(\frac{l^3\zeta^2\Lambda^2 C_1}{\epsilon^6} + \frac{l^3\Lambda^2 C_2}{\epsilon^4}\right)$ iterations with learning rate $\eta_\pi = \Theta(\epsilon^4/l^3\zeta^2\Lambda^2)$ and $\eta_{\boldsymbol{\lambda}} = \Theta(1/l)$ to converge to an ϵ-stationary point with convergence rate.

□

F Discussion

F.1 The Failure Case of State-Distance-Based Diversity Measures

A failure case of state-distance-based diversity measures may be when the state space includes many *irrelevant features*. These features cannot reflect behavioral differences. If we run SIPO in such an environment, the learned strategies may be only diverse w.r.t these features and have little visual distinction. Like the famous noisy TV problem [4], the issue of irrelevant features is intrinsically challenging for general RL applications, which cannot be resolved by using action-based or state-occupancy-based diversity measures either.

Thanks to the advantages we discussed in the paper, we generally find that state-distance-based measures can be preferred in challenging RL problems. Meanwhile, since the state dimension can be much higher than actions, it is possible that RL optimization over states may be accordingly more difficult than actions. In practice, we can design a feature selector for those most relevant features for visual diversity and run diversity learning over the filtered features. In SMAC and GRF, we utilize the agent features (excluding enemies) as the input of diversity constraint without further modifications, as discussed in Appendix D. We remark that even after filtering, the agent features remain high-dimensional while our algorithm still works well. Note that using a feature selector is a common practice in many existing domains, such as novelty search [11], exploration [29], and curriculum learning [6]. There are also works studying how to extract useful low-dimensional features from observations [63, 16], which are orthogonal to our focus.

F.2 The Distance Metric

In Sec. 5, we adopt the two most popular implementations in the machine learning literature, i.e., RBF kernel and Wasserstein distance, while it is totally fine to adopt alternative implementations. For example, we can learn state representations (e.g. auto-encoder, Laplacian, or successor feature) and utilize pair-wise distance or norms as a diversity measure. Similar topics have been extensively discussed in the exploration literature [63, 37]. We leave them as our future directions.

G Pseudocode of SIPO

The pseudocode of SIPO is shown in Algorithm 1.

Algorithm 1 SIPO (red for SIPO-RBF and blue for SIPO-WD)

Input: Number of Iterations M, Number of Training Steps within Each Iteration T.

Hyperparameter: Learning Rate η_π, Diversity Threshold δ, Intrinsic Scale Factor α, Lagrange Multiplier Upperbound λ_{max}, Lagrange Learning rate η_λ, Wasserstein Critic Learning Rate η_W, RBF Kernel Variance σ.

```
Archived trajectories $X \leftarrow \emptyset$                    // to store states visited by previous policies
for iteration $i = 1, \dots, M$ do
    Initialize policy $\pi_{\theta_i}$                                // initialization
    Initialize Wasserstein critic $f_{\phi_i}$
    for archive index $j = 1, \dots, i-1$ do
        Lagrange multiplier $\lambda_j \leftarrow 0$
    end for
    for Training step $t = 1, \dots, T$ do
        Collect trajectory $\tau = \{(s_h, \boldsymbol{a}_h, r(s_h, \boldsymbol{a}_h))\}_{h=1}^{H}$
        for archive index $j = 1, \dots, i-1$ do
            $R^j_{\text{int}} \leftarrow 0$
        end for
        for timestep $h = 1, \dots, H$ do
            $r_{\text{int},h} \leftarrow 0$                                 // compute intrinsic reward
            for archive trajectory $\chi_j \in X$ do
                $r^j_{\text{int},h} \leftarrow -\frac{1}{H|\chi_j|}\sum_{s'\in\chi_j} \exp\left(-\frac{\|s_h - s'\|^2}{2\sigma^2}\right)$
                $r^j_{\text{int},h} \leftarrow \frac{1}{H}\left[f_{\phi_j}(s_h) - \frac{1}{|\chi_j|}\sum_{s'\in\chi_j} f_{\phi_j}(s')\right]$
                $r_{\text{int},h} \leftarrow r_{\text{int},h} + \lambda_j \cdot r^j_{\text{int},h}$
                $R^j_{\text{int}} \leftarrow R^j_{\text{int},h} + r^j_{\text{int},h}$
            end for
            $r_h \leftarrow r(s_h, \boldsymbol{a}_h) + \alpha \cdot r_{\text{int},h}$
        end for
        for archive index $j = 1, \dots, i-1$ do
            $\lambda_j \leftarrow \text{clip}\left(\lambda_j + \eta_\lambda\left(-R^j_{\text{int}} + \delta\right),\ 0,\ \lambda_{\text{max}}\right)$        // gradient ascent on $\lambda_j$
            $\phi_j \leftarrow \phi_j + \eta_W \frac{1}{H}\sum_{h=1}^{H} \nabla_{\phi_j}\left(f_{\phi_j}(s_h) - \frac{1}{|\chi_j|}\sum_{s'\in\chi_j} f_{\phi_j}(s')\right)$
            $\phi_j \leftarrow \text{clip}(\phi_j, -0.01, 0.01)$
        end for
        Update $\pi_{\theta_i}$ with $\{(s_h, \boldsymbol{a}_h, r_h)\}$ by PPO algorithm          // policy gradient on $\theta_i$
    end for
    Collect many trajectories $\chi_i$                  // collect trajectories to approximate $d_{\pi_{\theta_i}}$
    $X \leftarrow X \cup \{\chi_i\}$                             // for the use of following iterations
end for
```